

RESEARCH ARTICLE

Nuclear m⁶A reader YTHDC1 regulates alternative polyadenylation and splicing during mouse oocyte development

Seth D. Kasowitz¹*, Jun Ma^{1,2}*, Stephen J. Anderson², N. Adrian Leu¹, Yang Xu¹, Brian D. Gregory², Richard M. Schultz^{2,3}, P. Jeremy Wang¹*

1 Department of Biomedical Sciences, University of Pennsylvania, Philadelphia, United States of America, **2** Department of Biology, University of Pennsylvania, Philadelphia, United States of America, **3** Department of Anatomy, Physiology and Cell Biology, School of Veterinary Medicine, University of California, Davis, Davis, United States of America

* These authors contributed equally to this work.

* pwang@vet.upenn.edu



OPEN ACCESS

Citation: Kasowitz SD, Ma J, Anderson SJ, Leu NA, Xu Y, Gregory BD, et al. (2018) Nuclear m⁶A reader YTHDC1 regulates alternative polyadenylation and splicing during mouse oocyte development. *PLoS Genet* 14(5): e1007412. <https://doi.org/10.1371/journal.pgen.1007412>

Editor: Wei Yan, University of Nevada School of Medicine, UNITED STATES

Received: February 22, 2018

Accepted: May 14, 2018

Published: May 25, 2018

Copyright: © 2018 Kasowitz et al. This is an open access article distributed under the terms of the [Creative Commons Attribution License](https://creativecommons.org/licenses/by/4.0/), which permits unrestricted use, distribution, and reproduction in any medium, provided the original author and source are credited.

Data Availability Statement: Oocyte RNA-seq data are available under the NCBI/SRA number: SRP116737.

Funding: This work was supported by National Institutes of Health/National Institute of General Medical Sciences grant R35GM118052 (to PJW), NIH/National Institute of Child Health and Human Development grant R01HD022681 (to RMS), and National Science Foundation (NSF) grant MCB-1623887 (to BDG). YX is supported by the Lalor foundation postdoctoral fellowship. The funders

Abstract

The N⁶-methyladenosine (m⁶A) modification is the most prevalent internal RNA modification in eukaryotes. The majority of m⁶A sites are found in the last exon and 3' UTRs. Here we show that the nuclear m⁶A reader YTHDC1 is essential for embryo viability and germline development in mouse. Specifically, YTHDC1 is required for spermatogonial development in males and for oocyte growth and maturation in females; *Ythdc1*-deficient oocytes are blocked at the primary follicle stage. Strikingly, loss of YTHDC1 leads to extensive alternative polyadenylation in oocytes, altering 3' UTR length. Furthermore, YTHDC1 deficiency causes massive alternative splicing defects in oocytes. The majority of splicing defects in mutant oocytes are rescued by introducing wild-type, but not m⁶A-binding-deficient, YTHDC1. YTHDC1 is associated with the pre-mRNA 3' end processing factors CPSF6, SRSF3, and SRSF7. Thus, YTHDC1 plays a critical role in processing of pre-mRNA transcripts in the oocyte nucleus and may have similar non-redundant roles throughout fetal development.

Author summary

The N⁶-methyladenosine (m⁶A) modification, one type of RNA methylation, is the most abundant internal RNA modification in eukaryote messenger RNAs. m⁶A is specifically recognized by RNA-binding reader proteins. Here we report an essential role of the nuclear m⁶A reader, YTHDC1, in embryo development and fertility. In particular, YTHDC1 is required for oocyte growth and maturation. YTHDC1-deficient oocytes exhibit massive defects in alternative splicing, which can be rescued by introducing into mutant oocytes wild-type, but not m⁶A-binding-deficient, YTHDC1. Strikingly, loss of YTHDC1 causes extensive alternative polyadenylation in oocytes, resulting in altered 3' UTR length. YTHDC1 interacts with the pre-mRNA 3'end processing factors CPSF6,

had no role in study design, data collection and analysis, decision to publish, or preparation of the manuscript.

Competing interests: The authors have declared that no competing interests exist.

SRSF3, and SRSF7. Thus, YTHDC1 is a key nuclear factor in the processing of pre-mRNA transcripts.

Introduction

More than one hundred different RNA modifications are known in eukaryotes [1]. N^6 -methyladenosine (m^6A) is the most prevalent internal modification in eukaryote mRNAs, occurring in transcripts of approximately one third of genes in human and mouse [2–4]. Globally, m^6A is enriched in the 3' most exons, long internal exons, and 5' untranslated regions (UTRs) [5–9]. In addition to mRNAs, m^6A is also present in long non-coding RNAs such as *Xist*, small nuclear RNAs, and ribosomal RNAs [10–12]. The m^6A RNA modification is widely conserved among eukaryotes including yeast, flies, and plants [13–17].

Generation of m^6A is catalyzed by a multi-component methyltransferase (m^6A writer) consisting of methyltransferase-like 3 (METTL3), methyltransferase-like 14 (METTL14), and Wilm's tumor associated protein (WTAP) [8, 18–20]. m^6A is a reversible modification and two m^6A demethylases have been identified: fat mass and obesity-associated protein (FTO) and alkB homolog 5 (ALKBH5) [21, 22]. Readers of the m^6A mark preferentially bind to m^6A and elicit downstream functions. Five mammalian m^6A readers contain the YTH (YT521-B homology) domain: YTHDF1, 2, 3 and YTHDC1, 2 [6, 23–26]. YTHDF1, 2, and 3 are cytoplasmic [6, 23]. YTHDC1 localizes to the nucleus in cultured mammalian somatic cells [27, 28], whereas YTHDC2 is cytoplasmic in meiotic spermatocytes [29–33]. The m^6A modification occurs preferentially at the conserved RRACH motif (R: G or A; H: A, C, or T) [34]. The YTH domain is an RNA-binding motif [35] and crystal structural studies reveal that the YTH domain of YTHDC1 selectively binds to m^6A in the consensus motif [24, 25]. In addition to the five YTH domain-containing m^6A readers, a number of RNA-binding proteins lacking a YTH domain are m^6A readers: IGF2BP proteins [36], FMR1 [37], the translation initiation factor eIF3 complex [38], HNRNPA2B1 [39, 40], HNRNPC [41], and HNRNPG [42]. The HNRNP family members are considered “indirect” m^6A readers, because m^6A alters the local RNA structure to facilitate their binding to m^6A [4, 40–42].

m^6A functions in key RNA metabolic processes. m^6A regulates gene expression [5, 6], mRNA stability [23, 43], translation efficiency [44, 45], alternative splicing [15, 16, 46], and cytoplasmic mRNA turnover [23, 47]. m^6A is also involved in a number of developmental processes. In yeast, m^6A formation occurs only during meiosis and is catalyzed by IME4, which is the sequence homologue of mammalian METTL3 and induces meiosis [13, 14]. m^6A modulates alternative splicing of *Sxl* (sex lethal) transcript and thus sex determination in *Drosophila* [15, 16]. m^6A is abundant on the long non-coding RNA *Xist* and promotes *Xist*-mediated gene silencing during X-inactivation [10]. Inactivation of *Mettl3* in mouse or *IME4* in *Drosophila* leads to embryonic lethality, demonstrating an essential role for m^6A in lineage differentiation [48, 49]. Mouse *Mettl3* is required for spermatogonial development and spermatogenesis [50, 51]. Disruption of the m^6A demethylase gene *Alkbh5* causes male infertility in mouse [22], whereas YTHDC2 is required for spermatogenesis and oogenesis in mouse [26, 31–33]. YTHDF2-mediated clearance of maternal transcripts promotes zygotic genome activation in zebrafish [52]. Mouse YTHDF2 regulates maternal transcript dosage and is essential for female fertility [53]. In addition, knockdown studies have uncovered a role of m^6A in zebrafish development [20], circadian rhythm [54], cell reprogramming [7, 49, 55], and miRNA biogenesis and effects [39, 56]. Therefore, m^6A plays important roles in a large number of developmental processes.

We previously identified YTHDC1 as a meiotic chromatin-associated protein in a proteomic screen [57]. YTHDC1 (initially referred to as YT521-B) changes alternative splicing patterns in a concentration-dependent manner [27] and localizes to nuclear speckles, which contain active transcription sites [28]. Tyrosine phosphorylation of YTHDC1 regulates its intra-nuclear localization, thereby modulating its effects on alternative splicing [58]. YTHDC1 promotes exon inclusion by recruitment of serine/arginine-rich (SR) splicing factor 3 (SRSF3), a pre-mRNA splicing factor [46]. YTHDC1 facilitates nuclear export of m⁶A-containing mRNAs through SRSF3 and NXF1 [59]. Although these studies in cultured cells have provided important insights into the function of YTHDC1, its requirement during development is unknown. In addition, the biological function of accumulation of m⁶A sites in 3' UTRs remains mysterious. Here, we report that YTHDC1 is essential for embryonic development in the mouse. Using a conditional inactivation approach, we find that YTHDC1 is required for survival of spermatogonia in males and controls postnatal oocyte development in females. Strikingly, in addition to alternative splicing defects, loss of YTHDC1 causes widespread alternative polyadenylation in oocytes. Importantly, YTHDC1 is associated with SR proteins and pre-mRNA 3' end processing factors.

Results

Nuclear localization of YTHDC1 in male germ cells, oocytes and pre-implantation embryos

We examined expression of YTHDC1 in adult mouse tissues using polyclonal antibodies raised against an N-terminal region of mouse YTHDC1 (S2A Fig). Western blot analysis showed that YTHDC1 was expressed in multiple adult mouse tissues including brain, testis, and ovary, with an apparent molecular weight of ~120 kDa (Fig 1A). High levels of YTHDC1 were present in postnatal oocytes, MII eggs, and pre-implantation embryos, and low levels in germinal vesicle (GV) stage oocytes (Fig 1B). The increase in YTHDC1 protein abundance between the GV oocyte stage and MII egg suggests that YTHDC1 is encoded by a dormant maternal mRNA that is recruited during oocyte maturation. Immunostaining showed that YTHDC1 localized to the nucleus in postnatal oocytes and pre-implantation embryos, with the increase in staining between the GV oocyte and MII egg being consistent with the immunoblotting results (Fig 1C). The diffuse cytoplasmic signal of YTHDC1 and its increased abundance in MII oocytes suggest that *Ythdc1* is under translational control, possibly in preparation for zygotic activation at the two-cell stage. The nuclear localization of YTHDC1 is consistent with a previous finding that it is associated with chromatin [57]. Notably, in postnatal day (PND) 5 and 12 oocytes, transcription is active and YTHDC1 is nuclear. In adult testis (S1 Fig), YTHDC1 is nuclear in spermatogonia, spermatocytes, and round spermatids, which are transcriptionally active. However, YTHDC1 is absent in elongating and elongated spermatids, which are transcriptionally inactive due to nuclear condensation (S1 Fig). Therefore, the nuclear localization of YTHDC1 in cells with active transcription suggests that it is involved in co-transcriptional and/or post-transcriptional regulations.

YTHDC1 is required for embryo viability

To determine the physiological function of *Ythdc1*, we generated a *Ythdc1* floxed (conditional) allele, referred to as *Ythdc1*^{fl}, by gene targeting in embryonic stem (ES) cells (S2B Fig). *Ythdc1*^{fl/fl} mice were healthy and fully fertile. We next crossed *Ythdc1*^{fl/fl} mice to *Actb-Cre* mice, which express Cre ubiquitously, to obtain mice with a *Ythdc1* null allele (*Ythdc1*^{+/-}) [60]. Cre-mediated excision of the floxed exons removes the YTH domain and causes a frameshift

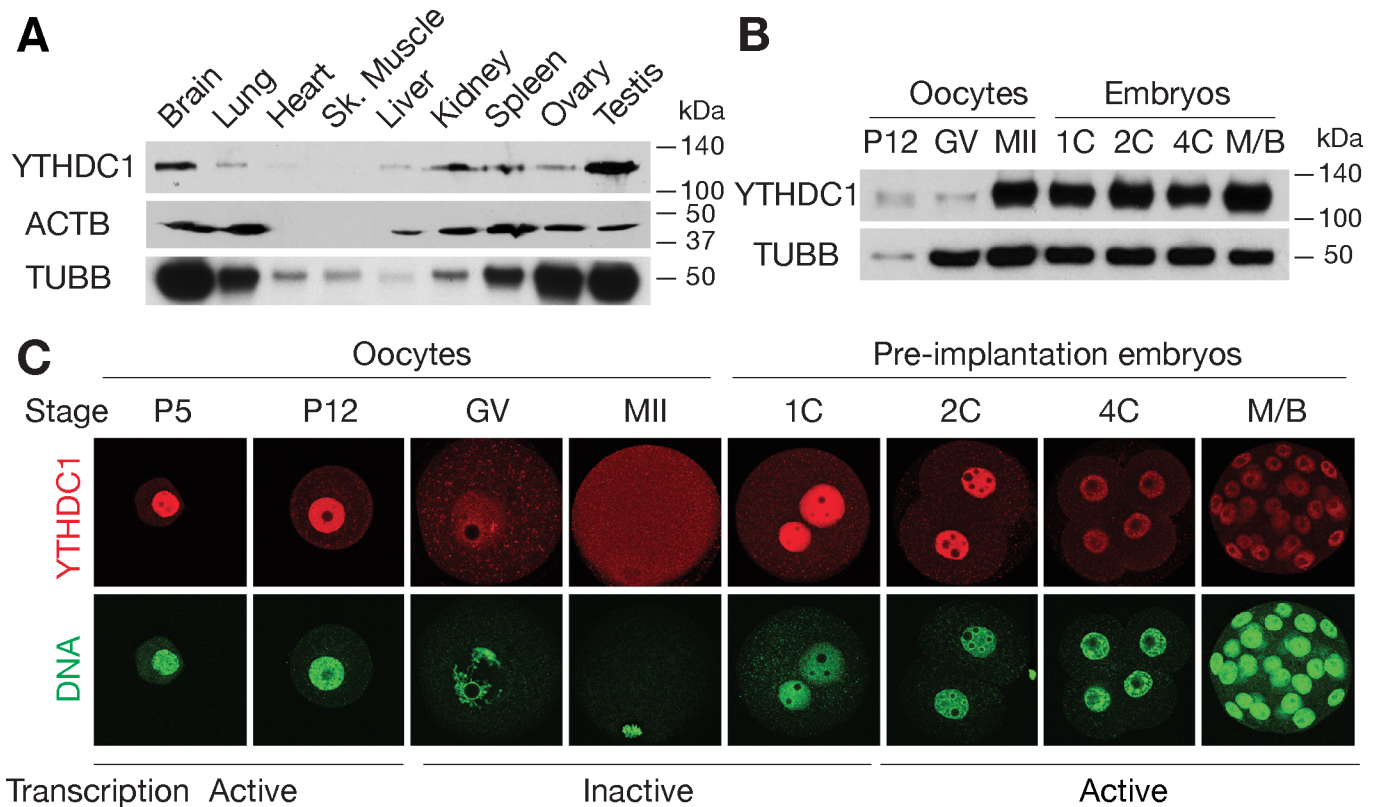


Fig 1. Expression and subcellular localization of YTHDC1 in oocytes and pre-implantation embryos. (A) YTHDC1 expression in adult mouse tissues. ACTB and TUBB (β -tubulin) served as loading controls. Heart and skeletal muscle contain little ACTB. (B) Western blot analysis of YTHDC1 in oocytes and pre-implantation embryos. TUBB served as a loading control. Note the lower levels of YTHDC1 in GV-stage oocytes, when normalized to TUBB. (C) Localization of YTHDC1 in oocytes and pre-implantation embryos. DNA was stained with Sytox green. Abbreviations: P5, P12: postnatal days 5, 12; GV, germinal vesicle stage; MII, metaphase II; 1C, 2C, 4C: 1-cell, 2-cell, 4-cell embryos; M/B, morula/blastocyst.

<https://doi.org/10.1371/journal.pgen.1007412.g001>

in the resulting *Ythdc1* mutant transcript (S2B Fig). Intercrosses of *Ythdc1*^{+/-} mice did not produce any *Ythdc1*^{-/-} pups, suggesting that *Ythdc1* is essential for embryonic development (S2C Fig). To determine the time of developmental failure, we genotyped fetuses recovered from intercrosses of *Ythdc1*^{+/-} mice at embryonic day 8.5 (E8.5), E9.5, and E11.5. No *Ythdc1*^{-/-} embryos were found at E11.5. Out of 9 embryos at E8.5 and out of 33 embryos at E9.5, only one *Ythdc1*^{-/-} embryo was found at each time point (S2C Fig). Resorbed embryos were found at E8.5 through E11.5 and expected to be homozygous mutants based on their Mendelian distribution (S2C Fig). These results show that YTHDC1 is indispensable for embryo development past early post-implantation stages.

YTHDC1 is essential for spermatogonium survival and male fertility

To bypass the embryonic lethality resulting from *Ythdc1* deficiency, we used *Ddx4*-Cre to inactivate *Ythdc1* specifically in the germline to generate *Ythdc1*^{fl/-} *Ddx4*-Cre (referred to as *Ythdc1*^{ckO}) mice (Figs 2 and 3A). All subsequent studies were conducted with *Ythdc1*^{fl/-} *Ddx4*-Cre (cKO) mice unless noted otherwise. *Ddx4*-Cre expression begins at ~E15 in both male and female germ cells but differs in the developmental stage of onset due to the sexual dimorphism in the timing of meiotic entry [61]. In males, *Ddx4*-Cre is expressed in mitotic germ cells including spermatogonia prior to meiosis, whereas in oocytes, *Ddx4*-Cre expression occurs only after meiotic entry (Fig 3A). *Ythdc1*^{ckO} mice were viable and grossly normal.

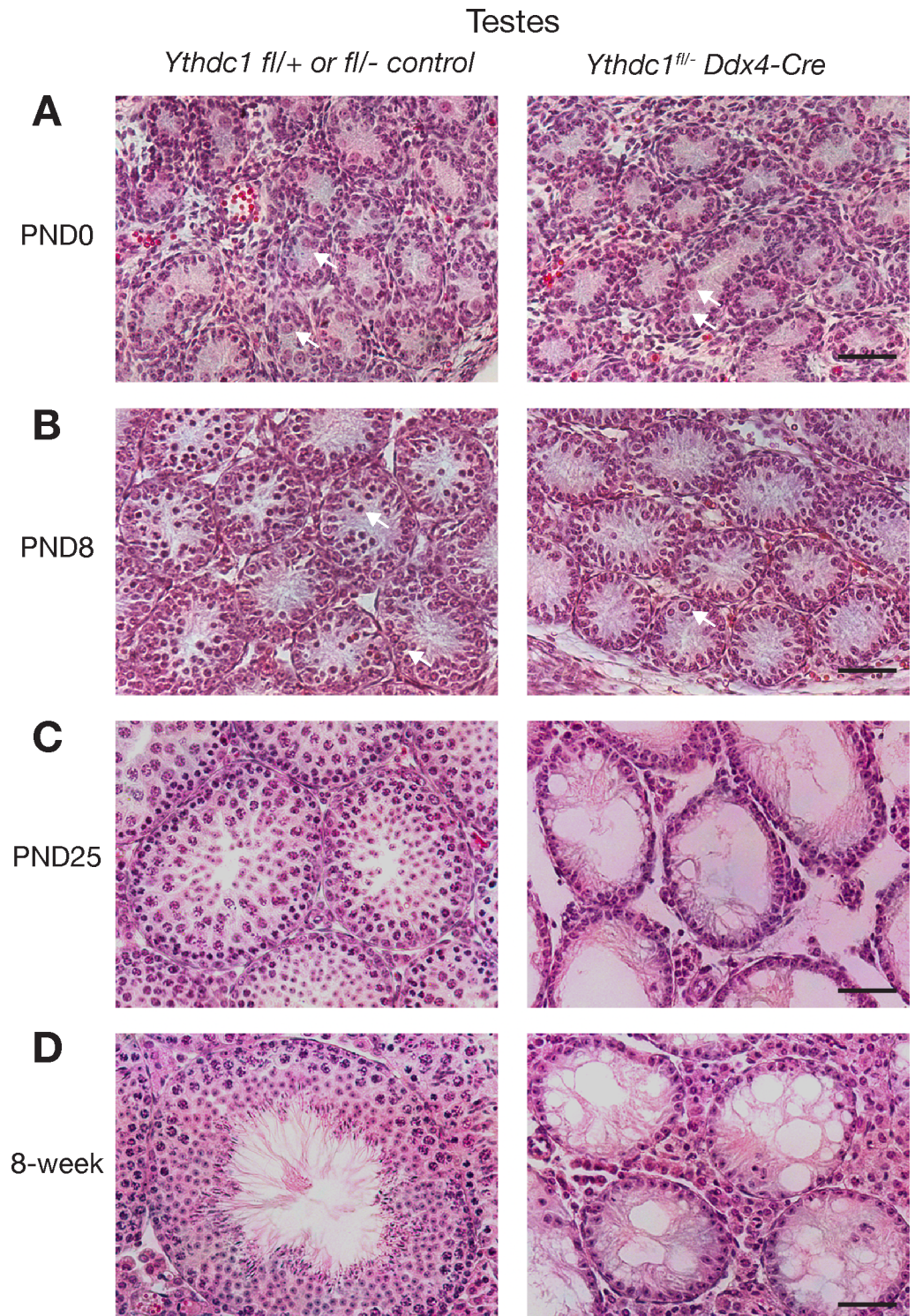


Fig 2. Postnatal loss of male germ cells in *Ythdc1*^{fl/-} Ddx4-Cre males. Histological analysis of testes from *Ythdc1* wild-type or heterozygous (left) and *Ythdc1*^{fl/-} Ddx4-Cre (right) males at birth (postnatal day 0) (A), PND8 (B), PND25 (C), and 8 weeks (D). Arrows in panels A and B indicate prospermatogonia and spermatogonia respectively. Scale bars, 50 μ m.

<https://doi.org/10.1371/journal.pgen.1007412.g002>

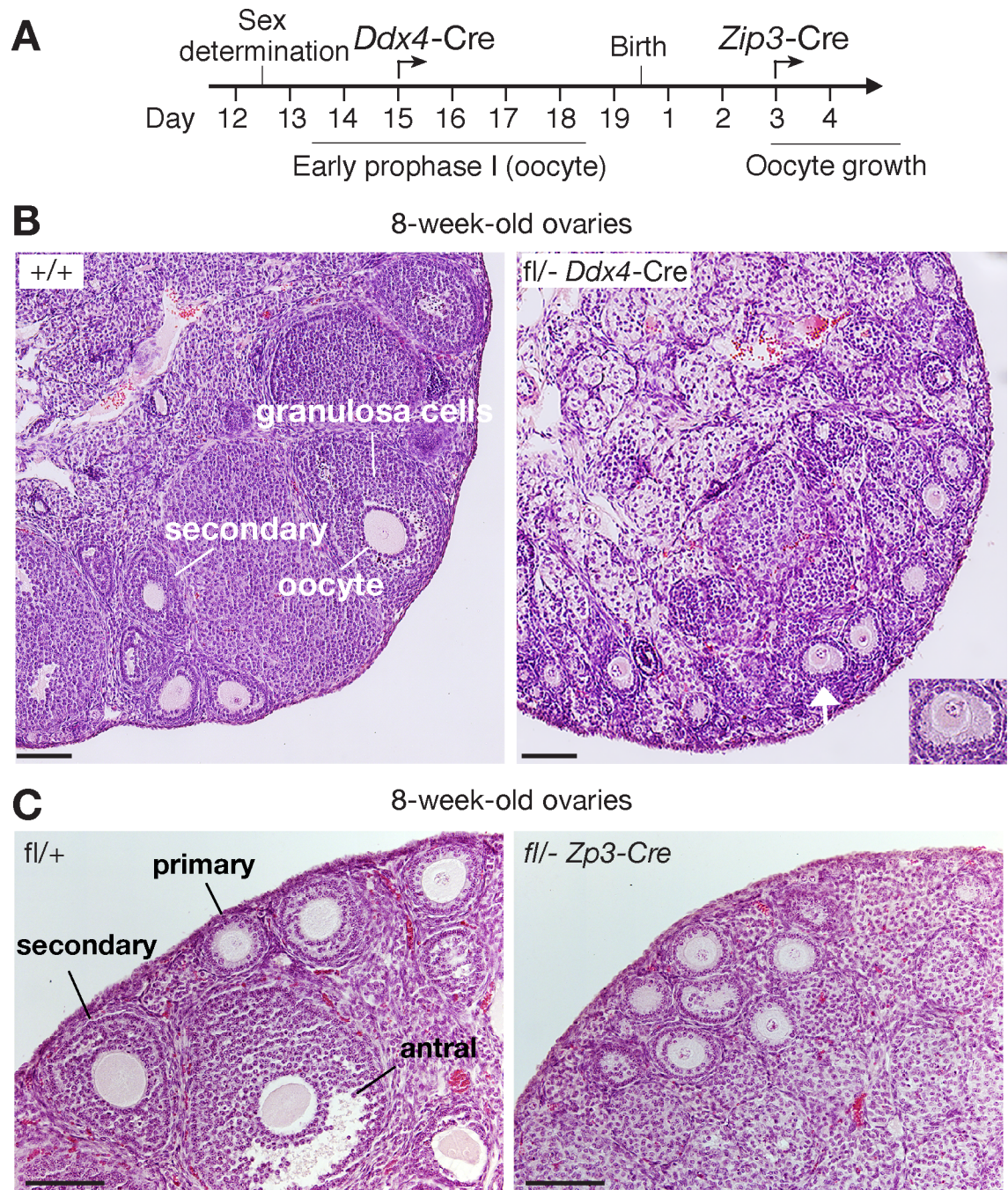


Fig 3. YTHDC1 is required for oocyte growth. (A) Timeline of disruption of *Ythdc1* in oocytes using *Ddx4-Cre* or *Zp3-Cre*. (B) Histological analysis of ovaries from 8-week-old wild-type and *Ythdc1^{fl/-} Ddx4-Cre* mice. Inset, enlarged view of the primary follicle marked by white arrow. Scale bars, 100 μ m. (C) Histological analysis of ovaries from 8-week-old wild-type and *Ythdc1^{fl/-} Zp3-Cre* mice. Scale bars, 100 μ m.

<https://doi.org/10.1371/journal.pgen.1007412.g003>

Seminiferous tubules from newborn (PND0) *Ythdc1^{CKO}* males contained prospermatogonia (Fig 2A), which lacked YTHDC1 as determined by immunostaining (S3 Fig). Tubules from PND8 *Ythdc1^{CKO}* males contained substantially fewer spermatogonia than those from control *Ythdc1^{fl/+}* or *Ythdc1^{fl/-}* males (Fig 2B). However, testes from PND25 and adult *Ythdc1^{CKO}*

males lacked any germ cells including mitotic spermatogonia and exhibited a Sertoli-cell-only phenotype (Fig 2C and 2D), demonstrating that *Ythdc1* is required for development of spermatogonia and male fertility.

Inactivation of YTHDC1 causes oocyte maturation arrest and female sterility

In contrast to the absence of germ cells in adult *Ythdc1* cKO testis, oocytes were present in ovaries from 8-week-old *Ythdc1^{fl/-} Ddx4-Cre* (cKO) females (Fig 3). Wild-type adult ovaries contained follicles at different developmental stages, including primary, secondary, and antral follicles (Fig 3B and 3C). However, *Ythdc1^{fl/-} Ddx4-Cre* ovaries lacked secondary or antral follicles, indicating that oocyte development was blocked at the primary follicle stage, which is characterized by one layer of granulosa cells surrounding the oocyte (Fig 3B). Histological analysis of ovaries from older *Ythdc1^{fl/-} Ddx4-Cre* females (6-month and beyond) showed a complete loss of oocytes. Western blot analysis confirmed that YTHDC1 protein was absent in oocytes collected from *Ythdc1^{fl/-} Ddx4-Cre* ovaries (S4A Fig). As expected, a nuclear immunofluorescent signal of YTHDC1 was not detected in *Ythdc1* mutant oocytes (S4B Fig). These results confirm the specificity of our YTHDC1 antibody and the complete depletion of YTHDC1 in *Ythdc1^{fl/-} Ddx4-Cre* oocytes.

Because expression of *Ddx4-Cre* begins at the pachytene stage of meiotic prophase I during fetal development, it is not clear whether the observed defects in *Ythdc1^{fl/-} Ddx4-Cre* postnatal ovaries were due to the requirement of YTHDC1 at embryonic or postnatal stages. To investigate whether postnatally expressed YTHDC1 is required for oocyte development, we used *Zp3-Cre* to inactivate *Ythdc1* in oocytes postnatally (Fig 3A). *Zp3-Cre* is expressed in developing oocytes around postnatal day 3 (Fig 3A) [62]. We found that *Ythdc1^{fl/-} Zp3-Cre* ovaries exhibited similar defects in folliculogenesis as observed in *Ythdc1^{fl/-} Ddx4-Cre* ovaries—blockade at the primary follicle stage (Fig 3C). We next performed mating tests of three *Ythdc1^{fl/-} Zp3-Cre* females and three wild-type littermate control females. At the age of 8 weeks, each female was housed with one wild-type male for two months. The three control females produced two litters each (6.8 ± 1.4 pups/litter), whereas none of the three *Ythdc1^{fl/-} Zp3-Cre* females produced any offspring. Taken together, these genetic studies demonstrate that YTHDC1 plays an essential role in postnatal oocyte development.

Ythdc1-deficient oocytes contain large cytoplasmic RNA granules

We were able to retrieve oocytes from ovaries of *Ythdc1^{fl/-} Ddx4-Cre* females at the ages of 3–6 weeks by poking. However, the number of oocytes retrieved from *Ythdc1^{fl/-} Ddx4-Cre* females was only 10% ($n = 3$) that of wild-type littermates. In addition, the GV oocytes from *Ythdc1^{fl/-} Ddx4-Cre* females were not able to resume meiosis in vitro. In contrast to the smooth appearance of wild-type germinal vesicle (GV) stage oocytes, *Ythdc1*-deficient oocytes contained one or two prominent granules in the cytoplasm (Fig 4A). Such granules were not observed in wild-type oocytes. These granules stained positive with Sytox green, which recognizes both DNA and RNA, suggesting a nucleic acid content (Fig 4B). When double stained with both DAPI and Sytox green, the nuclei of *Ythdc1*-deficient oocytes were positive for both stains, whereas the granules only retained the Sytox green stain, indicating that the granules contained RNA but not DNA (Fig 4B). To our knowledge, such large RNA granules have not been observed before. The appearance of large cytoplasmic RNA granules indicates severe defects in RNA metabolism in oocytes in the absence of YTHDC1. It is possible that, like P granules, incorrectly processed RNAs are sequestered in these novel RNA granules in oocytes in the absence of YTHDC1. Knockdown of YTHDC1 in HeLa cells causes acute nuclear

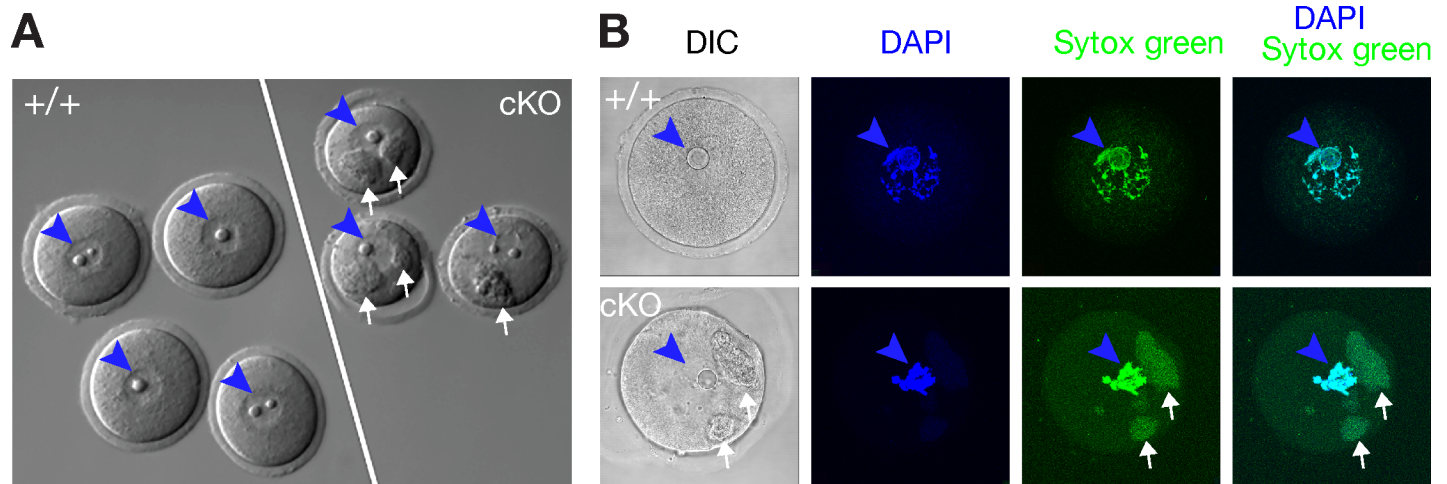


Fig 4. RNA-containing cytoplasmic granules in *Ythdc1*-deficient oocytes. (A) Presence of large cytoplasmic granules in oocytes from 11-week-old *Ythdc1*^{fl/fl} *Ddx4*-Cre (cKO) females. (B) Cytoplasmic granules in oocytes from 11-week-old *Ythdc1*^{fl/fl} *Ddx4*-Cre females contain RNA. Nuclei/nuclear DNA and cytoplasmic RNA granules are marked by arrowheads (blue) and arrows (white), respectively. DAPI stains DNA only. Sytox green stains both DNA and RNA.

<https://doi.org/10.1371/journal.pgen.1007412.g004>

accumulation of mRNAs within hours [59]. We did not observe nuclear accumulation of RNAs in postnatal *Ythdc1*-deficient oocytes, possibly because inactivation of *Ythdc1* begins at E15 (Fig 3A), weeks prior to our analysis.

To investigate the consequences of *Ythdc1* deficiency on the oocyte transcriptome, we performed RNA-seq analysis of oocytes collected from 6-week-old wild-type and *Ythdc1*^{fl/fl} *Ddx4*-Cre females (S1 Table). With a FDR cutoff of 0.01, a total of 4933 transcripts showed differential expression: 2656 transcripts were up-regulated and 2277 transcripts down-regulated in *Ythdc1*-deficient oocytes compared with control oocytes, indicating that the transcriptome in *Ythdc1*-deficient oocytes was dramatically altered (S5A Fig and S2 Table). Validation of 10 randomly selected differentially abundant transcripts by real-time PCR confirmed the RNA-seq findings (S5B Fig). Gene Ontology (GO) analysis identified a number of significantly altered biological processes for both up-regulated and down-regulated transcripts, with regulation of transcription as the most significantly affected process (S5C Fig).

Widespread splicing defects in *Ythdc1*-deficient oocytes

Because YTHDC1 affects alternative splicing in cultured somatic cells [27], we next analyzed the oocyte RNA-seq data to systematically identify local splicing variants (LSVs) between wild-type and *Ythdc1*-deficient oocytes using the MAJIQ package [63]. We identified a total of 2937 significant LSVs ($q < 0.05$) with Δ PSI (difference in percent spliced in) > 0.2 (Fig 5A and S3 Table). These LSVs affected 1966 genes, involved 10,266 exons, and included differential retention of 500 introns. Of the 1966 genes with LSVs, 34% (659 genes) were differentially expressed between wild-type and *Ythdc1*-deficient oocytes (up-regulated, 245 genes; down-regulated, 414 genes). According to GO analysis, these changes affect genes involved in multiple fundamental biological processes, including chromatin modification, regulation of transcription, mRNA processing, and regulation of translation (S6 Fig).

We designed RT-PCR assays to validate different types of MAJIQ-identified splicing events: exon inclusion/skipping, intron retention, and splicing in 3' UTRs. Using GV-stage oocytes from wild-type and *Ythdc1*^{fl/fl} *Ddx4*-Cre mice, RT-PCR analysis confirmed 90% (9 of 10 tested) of LSVs involving internal exons (Fig 5B and 5C). For example, as illustrated in the gene track

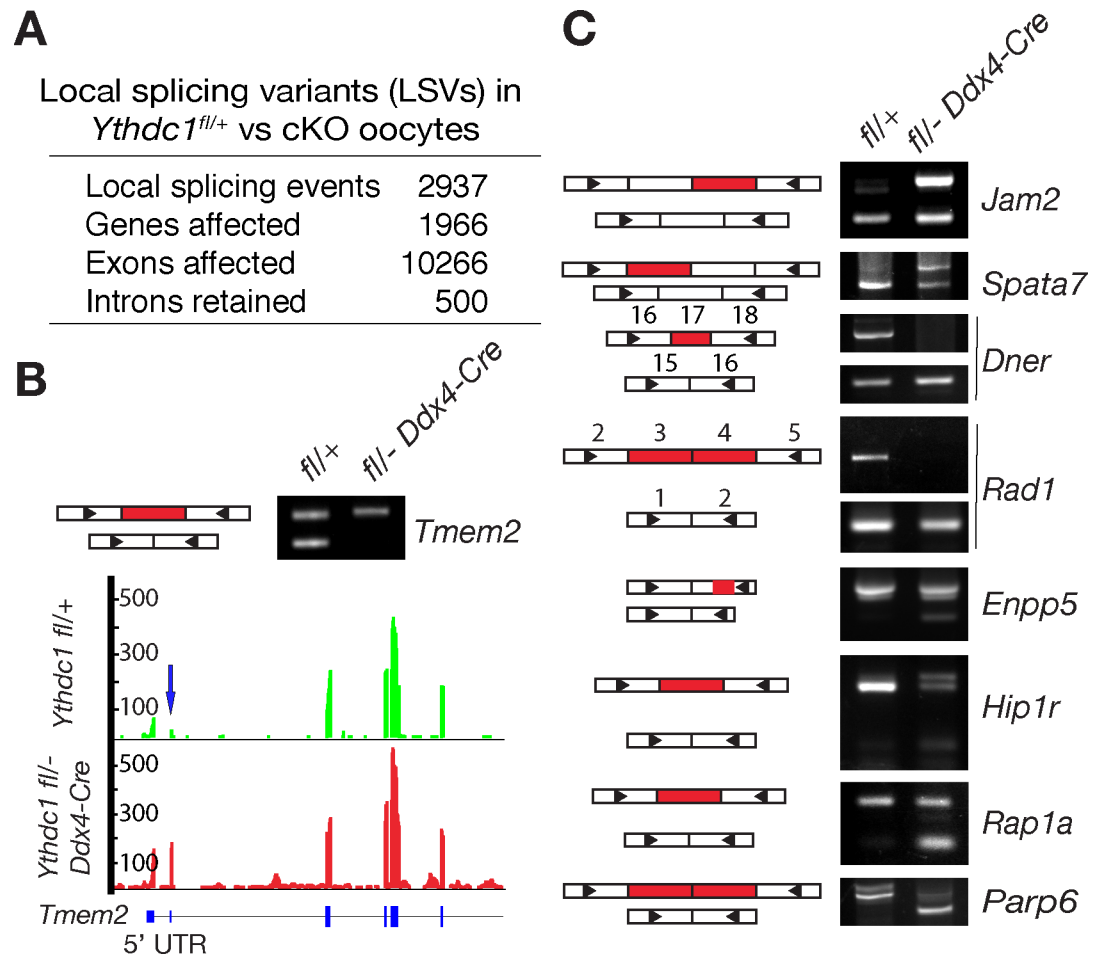


Fig 5. Changes in the splicing landscape in *Ythdc1*-deficient oocytes. Oocytes were collected from 6-week-old *Ythdc1*^{fl/+} and *Ythdc1*^{fl/-} *Ddx4*-Cre females. (A) Summary of local splicing variants (LSVs) identified by MAJIQ. Significant LSVs: ΔPSI (difference in percentage spliced in) > 0.2 and q < 0.05. (B) PCR validation and gene track view of one exon-skipping LSV in *Tmem2*. (C) PCR validation of LSVs affecting internal exons. Exons are represented as rectangles but not in scale. Skipped or retained exons are shown in red. Triangles denote the positions of PCR primers. Each PCR assays was performed three times using different samples.

<https://doi.org/10.1371/journal.pgen.1007412.g005>

view, the second exon (part of the 5'UTR) of *Tmem2* was partially skipped in wild-type but not in *Ythdc1*-deficient oocytes (Fig 5B). Two LSVs affecting *Jam2* and *Spata7*, respectively, involved nearly complete exon skipping in wild-type oocytes but partial exon skipping in *Ythdc1*-deficient oocytes. Exon skipping in two genes (*Dner* and *Rad1*) was complete in *Ythdc1*-deficient oocytes but partial in wild-type. Four LSVs in *Enpp5*, *Hip1r*, *Rap1a*, and *Parp6* resulted in partial exon skipping in *Ythdc1*-deficient oocytes whereas no skipping occurred in wild-type. There was no apparent preference for the directionality of exon skipping in regard to genotype. In total, our validation results suggest that most LSVs predicted by MAJIQ are true splicing events.

LSVs involving introns or 3' UTRs were more complex. We tested nine intron-retention LSVs predicted by MAJIQ and confirmed six of these (67%) by RT-PCR (Fig 6A and 6B). Among three confirmed LSVs, two transcripts (*Dnpep* and *McpH1*) showed intron retention preferentially in wild-type oocytes, whereas one mRNA (*Phf1*) retained introns preferentially in *Ythdc1*-deficient oocytes. We examined 13 MAJIQ-predicted LSVs involving splicing within

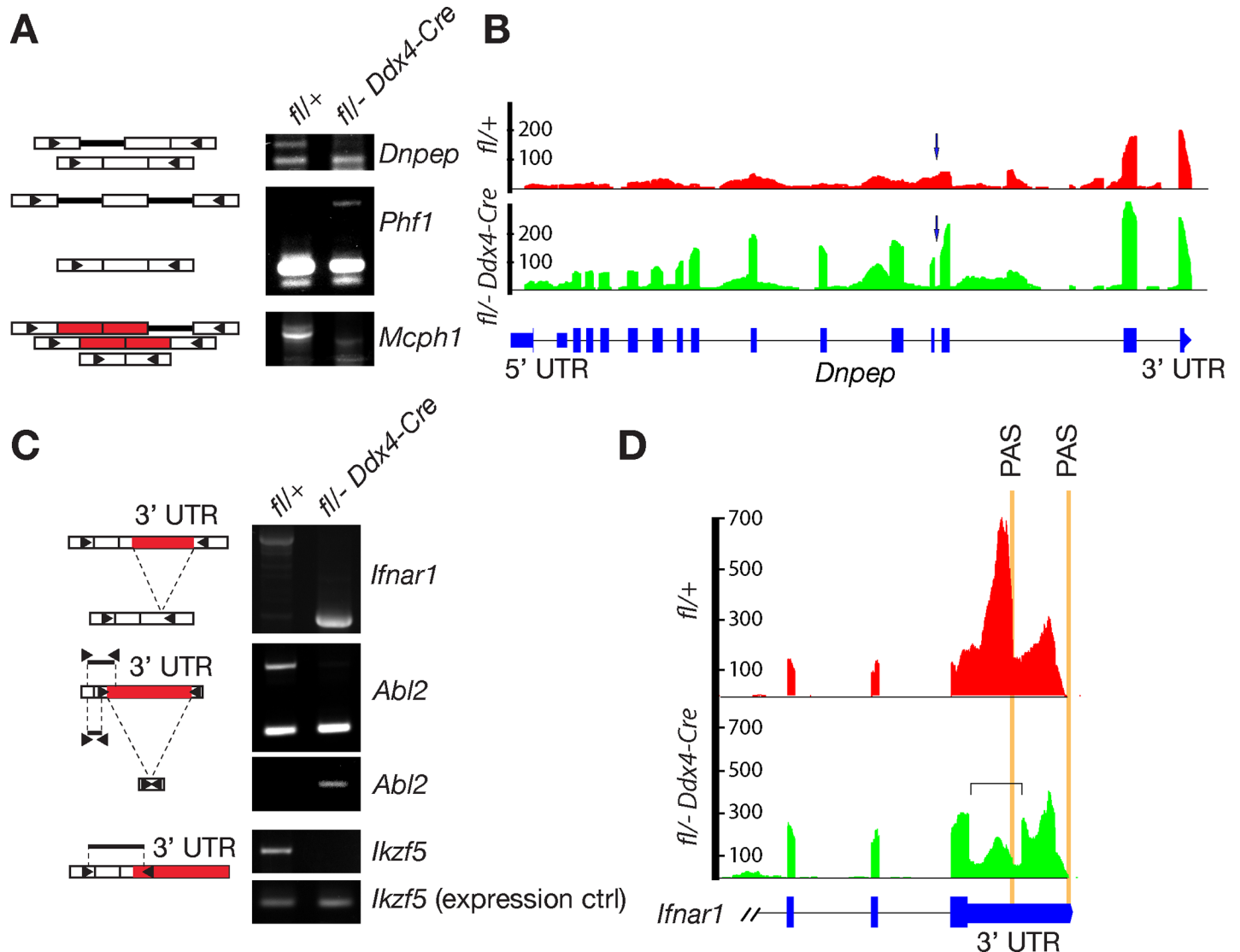


Fig 6. Local splicing variants involve intron retention and 3' UTR. Oocytes were collected from 6-week-old *Ythdc1*^{fl/+} and *Ythdc1*^{fl/-} *Ddx4-Cre* females. (A) PCR validation of intron-retaining LSVs. Introns and exons are represented as thick lines and rectangles, respectively. (B) Gene track view of a retained intron in the *Dnpep* Gene. Arrow indicates the affected intron. (C) PCR validation of LSVs in 3' UTRs. The affected portion of the respective 3' UTR is shown in red. Triangles denote the positions of PCR primers (A and C). (D) Gene track view of splicing variant in the *Ifnar1* 3' UTR. The square bracket demarcates the spliced region of 3' UTR in *Ythdc1*-deficient oocytes. Polyadenylation sites (PAS) are marked by vertical orange lines.

<https://doi.org/10.1371/journal.pgen.1007412.g006>

3' UTRs and validated three of these (23%) by RT-PCR (Fig 6C and 6D): *Ifnar1*, *Abl2*, and *Ikzf5*. Coincidentally, all of these transcripts were associated with longer 3' UTRs in wild-type oocytes. Although MAJIQ was not designed for the analysis of changes in introns and 3' UTR length as pointed out by the MAJIQ authors, we were able to validate most of the MAJIQ-predicted LSVs involving introns and some of the 3' UTR splicing events.

We further examined the 9 LSVs involving exon inclusion/skipping using GV-stage oocytes from 6-week-old *Ythdc1*^{fl/-} *Zp3-Cre* and wild-type females. All 9 LSVs validated in *Ythdc1*^{fl/-} *Ddx4-Cre* oocytes (Fig 5) were also confirmed in *Ythdc1*^{fl/-} *Zp3-Cre* oocytes (S7 Fig). Collectively, our results show that inactivation of YTHDC1 in oocytes causes severe defects in mRNA splicing.

Extensive alternative polyadenylation in *Ythdc1*-deficient oocytes

The majority of m⁶A sites are present in the 3' most exons, raising the possibility that m⁶A may play a role in regulating 3' UTR length [5, 9]. Many genes produce transcripts with 3' UTRs of different lengths due to usage of alternative polyadenylation (APA) sites and 3' UTRs contain sites for microRNAs and RNA-binding proteins. Thus, the 3' UTR of a particular mRNA regulates its translation and subcellular localization [64, 65]. For instance, transcripts in brain exhibit extensive lengthening of 3' UTRs due to APA [66]. We systematically analyzed the 3' UTR length of wild-type versus *Ythdc1*-deficient oocytes using the ROAR algorithm [67]. The ROAR program identifies alternative polyadenylation using standard RNA-seq data by measuring the reads upstream (pre) and downstream (post) of the annotated polyadenylation site (PAS) (Figs 7A and 6B). ROAR analysis of our oocyte RNA-seq data revealed 1210 alternative polyadenylation (APA) events in 864 genes between wild-type and *Ythdc1* mutant oocytes (cutoff, p value < 0.05; Fig 7A and S4 Table). Some genes had more than one differential APA event. Overall, 709 APA events (ROAR < 1) resulted in higher levels of the longer isoform (longer 3' UTR) in *Ythdc1*-deficient oocytes, whereas 501 APA events (ROAR > 1) was associated with higher levels of the shorter isoform in the mutant (Fig 7A).

We chose 8 transcripts with predicted longer 3' UTRs in the *Ythdc1* mutant for RT-PCR validation (Fig 7B). These 8 transcripts were not differentially expressed between wild-type and mutant oocytes. Our validation strategy involved one PCR assay (termed PRE) that amplified both short and long transcripts and a second PCR assay (termed POST) that was specific for the long isoform. The POST RT-PCR assay for *Arl5a* produced a stronger signal from *Ythdc1*-deficient versus wild-type oocytes, indicating that the former contained a higher level of the long isoform. Of the eight transcripts tested, seven (88%) (*Arl5a*, *Ddx21*, *Noc3l*, *Rybp*, *Scamp1*, *Slc11a2*, and *Slc25a51*) preferentially produced the longer isoform in *Ythdc1*-deficient oocytes due to APA, whereas, one transcript (*Frs2*) did not exhibit detectable differences in isoform prevalence using this assay (Figs 7C and 6D). These results demonstrate extensive alternative polyadenylation in *Ythdc1*-deficient oocytes. Previous findings in brain tissue [9] have shown that five of seven gene transcripts with APA defects contained known m⁶A sites in the last exons: *Arl5a*, *Ddx21*, *Noc3l*, *Slc11a2*, and *Slc25a51*, implicating m⁶A in regulation of alternative polyadenylation.

m⁶A-dependent rescue of alternative splicing defects in *Ythdc1*-deficient oocytes

To examine the effect of m⁶A on splicing in oocytes, we collected oocytes from wild-type and *Ythdc1*^{fl/-} *Ddx4*-Cre ovaries at postnatal day 12 (PND12), when oocytes are still transcriptionally active. We evaluated alternative splicing of the nine transcripts for which we had identified splicing defects in GV stage oocytes from 6-week-old *Ythdc1*^{fl/-} *Ddx4*-Cre mice (Fig 5) and found that all nine transcripts showed similar splicing defects in PND12 *Ythdc1*-deficient oocytes (Fig 8, first two lanes of center panel). However, there were notable differences for two transcripts: *Rad1* and *Tmem2*. The *Rad1* two-exon-skipping isoform was detected in PND12 mutant oocytes (Fig 8) but not in 6-week-old mutant oocytes (Fig 5). Similarly, the *Tmem2* spliced short isoform was present in PND12 mutant oocytes but absent in 6-week-old oocytes. These data suggest that the short isoforms of *Rad1* and *Tmem2* were degraded during the long period between cessation of transcription at PND20 and the time point of analysis at 6 weeks-of-age.

To investigate if alternative splicing defects in *Ythdc1*-deficient oocytes could be rescued by supplying YTHDC1, we used transcriptionally active PND12 oocytes. We injected PND12 *Ythdc1*-deficient oocytes with *in vitro* transcribed wild-type or mutant *Ythdc1* mRNA,

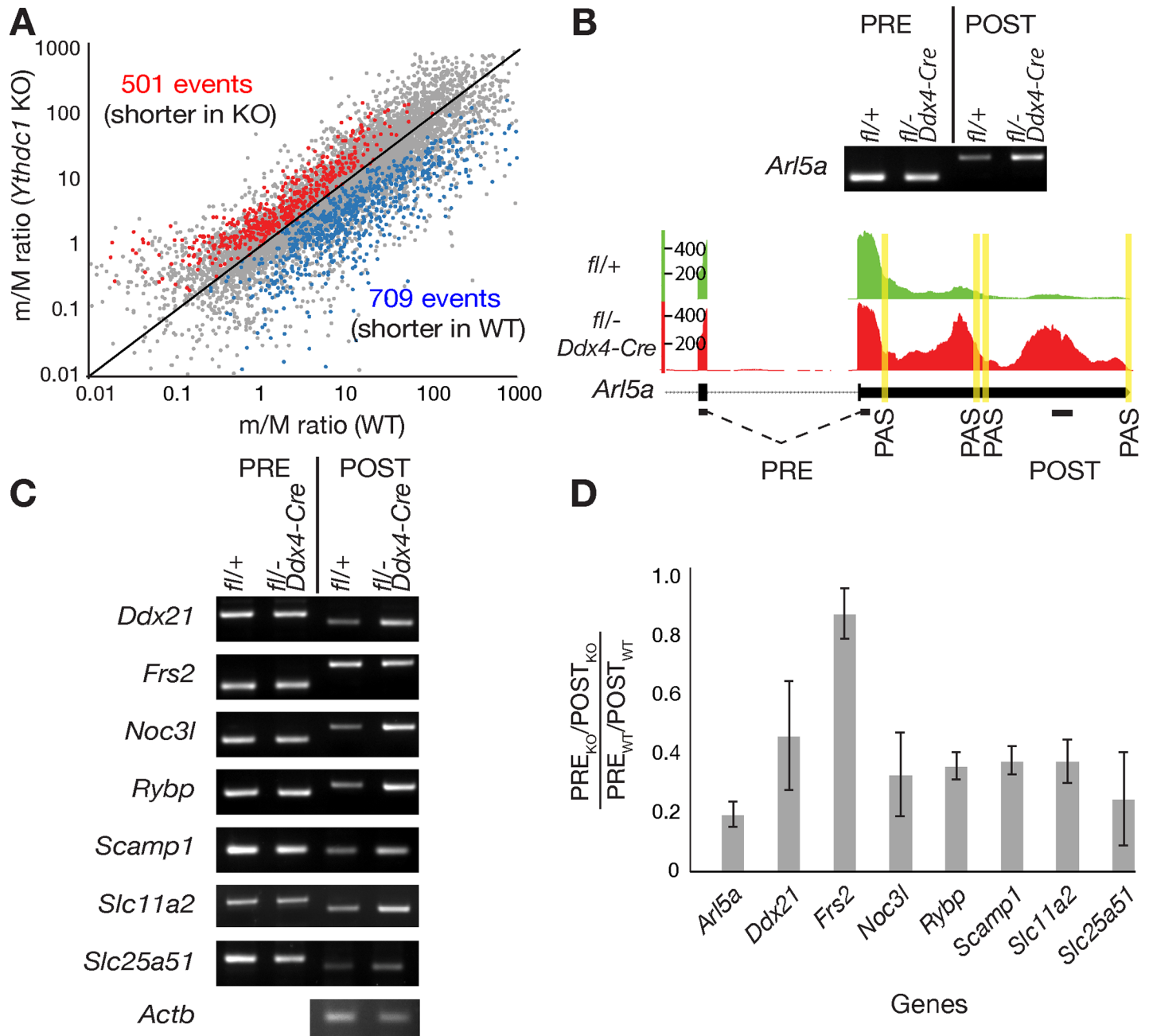


Fig 7. Alternative polyadenylation in *Ythdc1*-deficient oocytes. Oocytes were collected from 6-week-old *Ythdc1*^{fl/+} and *Ythdc1*^{fl/-} *Ddx4*-Cre females. (A) Pairwise comparison of PAS usage in wild-type and *Ythdc1*-deficient oocytes. PAS pairs with $p < 0.05$ are shown in red or blue. (B) Gene track view and RT-PCR validation of alternative polyadenylation in *Arl5a*. Polyadenylation sites (PAS) are marked by vertical yellow lines. Exons and introns are marked by black bars and dotted lines, respectively, and the location of PRE and POST PCR fragments is shown. (C) RT-PCR validation results of alternative polyadenylation in 7 genes. *Actb* served as a loading control. (D) Quantification of RT-PCR products of 8 genes shown in panels A and B. A ratio $[(PRE_{KO}/POST_{KO})/(PRE_{WT}/POST_{WT})]$ less than 1 indicates a higher level of the long isoform (with a longer 3' UTR) in *Ythdc1*-deficient oocytes. A ratio of 1 for *Frs2* indicates no preference between wild-type and mutant. Y-axis: mean \pm SD. The experiments were performed in triplicates.

<https://doi.org/10.1371/journal.pgen.1007412.g007>

followed by overnight culture. The *Ythdc1* mutant mRNA contains two missense mutations (W377A, W428A) that completely abolish the m⁶A binding activity of YTHDC1 [24]. We quantified the FLAG-YTHDC1 protein levels in the nucleus of injected *Ythdc1*-deficient

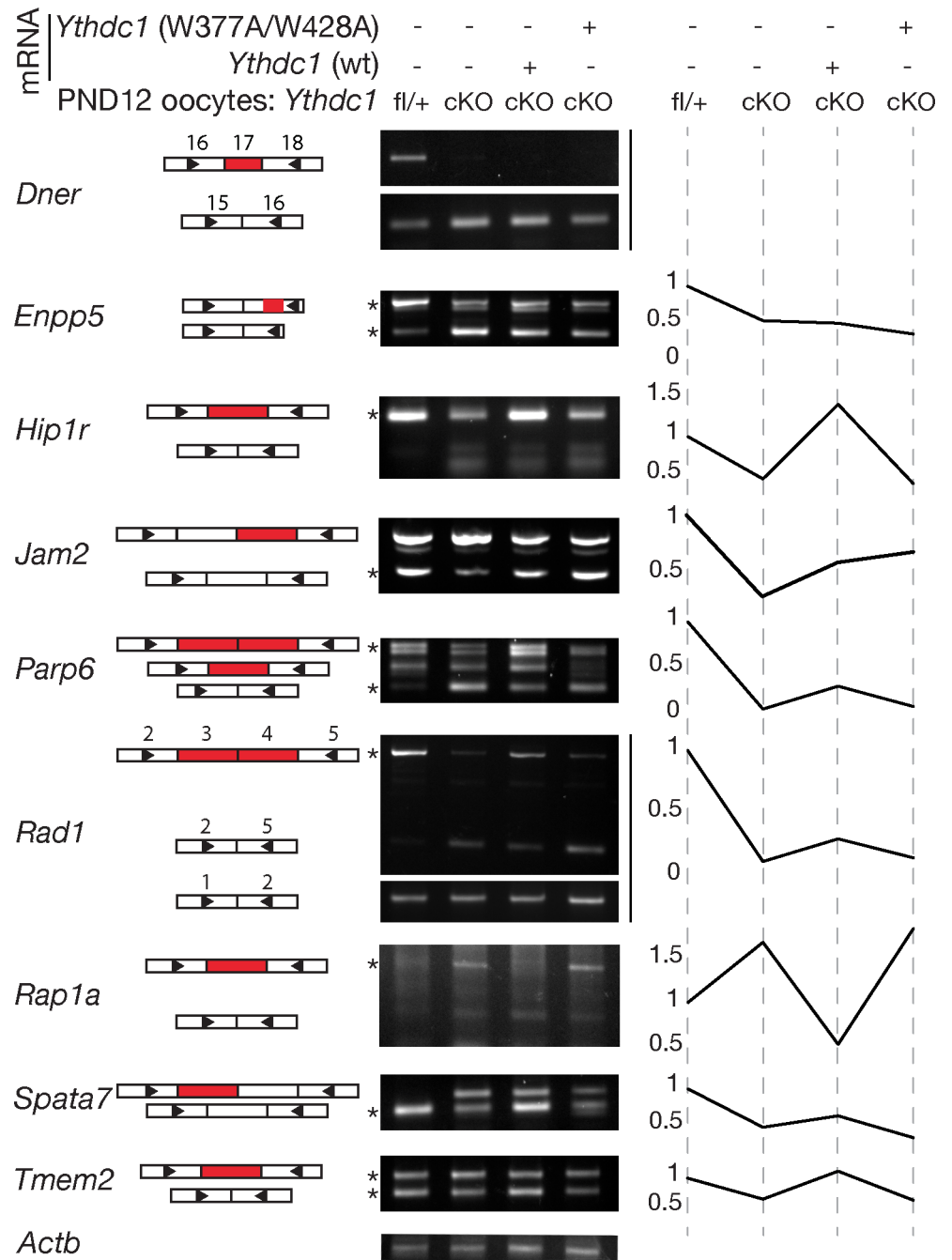


Fig 8. m⁶A-dependent rescue of alternative splicing defects in Ythdc1-deficient oocytes. Postnatal day 12 *Ythdc1*^{fl/+}-*Ddx4*-Cre (cKO) oocytes were injected with mRNAs encoding wild-type or m⁶A-binding-deficient mutant (W377A/W428A) YTHDC1 as marked on top of the gel panel, followed by RT-PCR analysis of LSVs. Left panel, schematic illustration of alternative splicing events for each transcript that correspond to the PCR products shown in the center panel. Each rectangle represents one exon, and exons subject to alternative splicing are marked red. Right panel, plot depicting quantification of ratios of band intensity or a single band intensity, with the value for wild-type oocyte (lane 1) set at 1. Asterisks indicate bands used for quantification. *Enpp5* and *Parp6*: ratio of the upper band / the lower band; *Tmem2*: ratio of the lower band / the upper band. *Actb* serves as a loading control.

<https://doi.org/10.1371/journal.pgen.1007412.g008>

oocytes by immunofluorescence and confocal microscopy and found no difference in

YTHDC1 protein levels between oocytes (4 oocytes each) injected with wild-type and mutant *Ythdc1* mRNAs. We found that exon skipping and exon inclusion defects in six transcripts were rescued in *Ythdc1*-deficient oocytes injected with wild-type but not mutant *Ythdc1* mRNA, whereas no difference was observed for the remaining three genes (*Dner*, *Enpp5* and *Jam2*) (Fig 8). These rescue experiments suggest that the majority of alternative splicing defects in *Ythdc1*-deficient oocytes is m⁶A-dependent. However, we cannot rule out the possibility that the failure of mutant YTHDC1 ((W377A, W428A) to rescue might be caused by reduced RNA-binding activity or instability, independent of m⁶A.

YTHDC1 interacts with pre-mRNA 3' end processing factors

To elucidate the mechanism by which YTHDC1 affects alternative polyadenylation, we investigated potential interactions of YTHDC1 with pre-mRNA 3' end cleavage and polyadenylation factors by co-immunoprecipitation (Fig 9). Cleavage factor Im (CFIm) and cleavage stimulating factor (CSTF) are two multi-protein complexes that bind to upstream sequence elements (USE) and downstream sequence elements (DSE) around the PAS, respectively [68, 69]. We found that YTHDC1 was associated with CPSF6, one of the four subunits of the CFIm complex (Fig 9A). This result is consistent with previous reports identifying CPSF6 among proteins co-immunoprecipitated with human YTHDC1 in 293T cells [46]. However, YTHDC1 did not interact with NUDT21, another subunit of the CFIm complex (Fig 9A). In addition, YTHDC1 was not associated with cleavage stimulating factors CSTF1 or CSTF2 by co-transfection and co-IP assays. Interestingly, knockdown of *Cpsf6* induces widespread use of proximal PAS, resulting in 3' UTR shortening [70, 71]. Moreover, a mutation in the Medaka *Cpsf6* gene causes 3' UTR shortening in developing embryos and a defect in primordial germ cell migration [72].

YTHDC1 interacts with the SR splicing factors SRSF3 and SRSF7 (Fig 9B). SRSF3 and SRSF7 couple RNA processing with mRNA export through association with the nuclear mRNA export factor NXF1 [73]. SRSF3 and SRSF7 bind to the last exons and regulate polyadenylation in an opposing manner. Knockdown of SRSF3 leads to 3' UTR shortening, whereas depletion of SRSF7 results in 3' UTR lengthening [73]. In conclusion, these results support a model in which YTHDC1 regulates alternative polyadenylation through interaction with the 3' end processing machinery.

Discussion

Here, we report that the nuclear m⁶A reader YTHDC1 is essential for mouse embryogenesis and germline development, and describe a critical role of YTHDC1 in orchestrating m⁶A-dependent processing of pre-mRNA transcripts in oocytes. Our studies implicate YTHDC1 in the choice of polyadenylation sites, which determines the length of 3' UTRs. The 3' UTR contains target sites for microRNAs and many RNA-binding proteins. Therefore, lengthening or shortening of 3' UTR would predictably have profound effects on translation efficiency, transcript stability, and subcellular transcript localization [64, 65, 68, 69]. Precise translational control of maternal transcripts is especially critical during oocyte maturation, due to lack of transcription during this prolonged stage. We find that loss of YTHDC1 in oocytes results in alternative polyadenylation and thus altered 3' UTR length in more than 800 genes. To date, YTHDC1 is the only m⁶A reader that has been demonstrated to regulate 3' UTR length.

Triple knockdown of three m⁶A writer components (METTL3, METTL14, and WTAP) in human A549 cells changes the usage of proximal versus distal polyadenylation sites with some switching to proximal sites and others switching to distal sites, demonstrating a critical role for m⁶A in regulation of 3' UTR length [9]. In addition, ALKBH5, an m⁶A demethylase, regulates

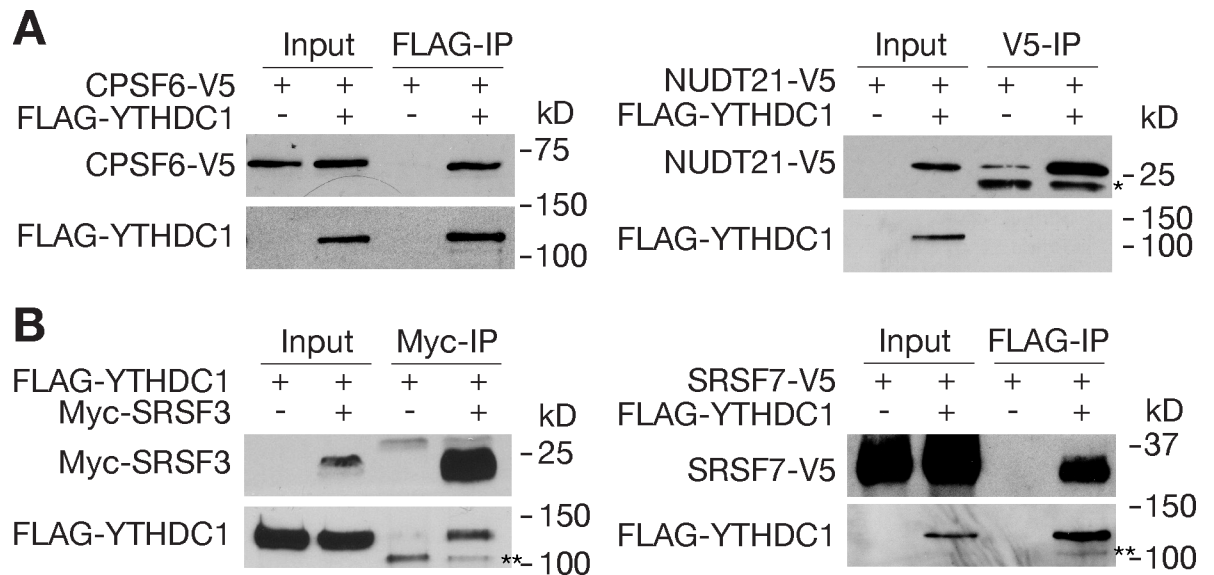


Fig 9. Association of YTHDC1 with pre-mRNA 3' end processing factors. Recombinant proteins were expressed in HEK 293T cells. Co-immunoprecipitation was carried out in the presence of RNase. (A) Co-IP analysis of YTHDC1 with CPSF6 and NUDT21. * indicates antibody light chain. (B) Co-IP analysis of YTHDC1 with SRSF3 and SRSF7. ** indicates a non-specific band.

<https://doi.org/10.1371/journal.pgen.1007412.g009>

3'UTR length in male germ cells [74]. How the m⁶A signal is relayed to the 3' end processing machinery is unknown. A number of multi-protein complexes participate in pre-mRNA 3' end cleavage and polyadenylation, including cleavage factor Im (CFIm), cleavage and polyadenylation specificity factor (CPSF), cleavage stimulating factor (CSTF), and poly(A)-binding proteins [68, 69]. We find that YTHDC1 forms complexes with components of the 3' end processing machinery: CPSF6 (a CFIm component), SRSF3, and SRSF7 (Fig 9). These factors bind to the 3' UTR around the PAS. Specifically, the CFIm binds to the UGUA motif upstream of the PAS. Knockdown of each of these factors in cell culture causes a shift in PAS usage, resulting in APA. Knockdown of CPSF6 favors usage of proximal PAS [70, 71], whereas knockdown of SRSF7 causes preferential usage of distal PAS [73]. Our data support a model in which YTHDC1 recognizes m⁶A in the last exons of pre-mRNA transcripts and orchestrates the choice of polyadenylation sites through interactions with 3' end processing factors. YTHDC1 may recruit these factors to the 3' UTRs or sequester them in the nucleoplasm through interactions, resulting in opposing APA patterns. Alternatively, these factors may compete for binding to YTHDC1. In addition, SRSF3 and SRSF7 link alternative polyadenylation with nuclear export through interaction with NXF1 [73]. Therefore, it is conceivable that, through interaction with SRSF3 and SRSF7, YTHDC1 may couple m⁶A in alternatively polyadenylated transcripts with nuclear export. In cultured cells, YTHDC1 facilitates binding of m⁶A-modified nuclear transcripts to SRSF3 and NXF1 and mediates nuclear export [59].

Our study reveals an essential role for YTHDC1 in development of both the embryo and the germline. Proteins (writers, readers, and erasers) involved in establishment, recognition, and erasure of m⁶A sites in mRNAs play important roles in development and fertility in mouse. Loss of the key m⁶A writer enzyme METTL3 causes early post-implantation lethality with defects in lineage priming [49]. m⁶A mainly reduces mRNA stability in embryonic stem cells and pre-implantation embryos and its loss leads to a failure in termination of naïve pluripotency during lineage specification [49]. Conditional inactivation of *Mettl3/Mettl14* reveals their essential role in spermatogenesis [50, 51]. *Alkbh5*-deficient mice are viable but exhibit

impaired spermatogenesis with increased apoptosis of meiotic spermatocytes [22]. ALKBH5-mediated m⁶A demethylation affects mRNA export. The cytoplasmic m⁶A reader YTHDC2 interacts with the meiosis-specific protein MEIOC [29, 30]. *Ythdc2*-deficient mice are viable but sterile due to a failure in meiotic progression [26, 31–33]. YTHDC2 together with MEIOC promotes translation efficiency of its target transcripts but decreases their mRNA abundance. In addition, YTHDC2 modulates the level of m⁶A-enriched transcripts in germ cells, which is required for progression through meiosis [32]. *Ythdf2* deficiency causes incomplete penetrance of lethality and female-specific infertility [53].

Similar to *Mettl3*, inactivation of *Ythdc1* is embryonic lethal, showing that loss of YTHDC1 is not compensated for by other m⁶A readers. The lack of compensation is not entirely surprising, given that, to date, YTHDC1 is the only known m⁶A reader in the nucleus. By conditional inactivation of *Ythdc1* in the germline, we find that YTHDC1 is essential for fertility in both males and females. Specifically, YTHDC1 is required for development of mitotic spermatogonia in males and oocyte growth in females. Because of loss of spermatogonia in *Ythdc1*^{fl/-} *Ddx4*-Cre males, different Cre drivers will be needed to examine its role in meiotic spermatocytes and post-meiotic round spermatids in future studies. Strikingly, the mouse mutant phenotypes of three m⁶A readers YTHDC1, YTHDC2, and YTHDF2 are different, suggesting non-redundant functions. YTHDC2 is required for meiotic progression in both sexes but is dispensable for viability [26, 31–33]. YTHDF2 is partially necessary for viability and specifically required for female fertility and oocyte competence [53]. Here we find that YTHDC1 is essential for viability and is required for spermatogonial development in males and oocyte growth in females. About 200 transcripts were upregulated in *Ythdf2*-deficient MII oocytes [53]. The overlap between the upregulated transcripts in *Ythdf2*-deficient oocytes and *Ythdc1*-deficient oocytes is significant (1.48-fold enrichment, $p = 0.0004$), suggesting that YTHDC1 may play a later role in oocyte competence. In *Ythdc1*^{fl/-} *Ddx4*-Cre or *Ythdc1*^{fl/-} *Zp3*-Cre females, germ cells progress through the prophase of meiosis I, however, oocyte development is blocked at the primary follicle stage. This blockade is similar to the oocyte growth arrest in females lacking GDF9, a key TGF β receptor ligand [75].

Several early studies using cultured cells show that YTHDC1 is involved in alternative splicing of internal exons in a dosage-dependent manner [27, 28, 58]. YTHDC1 localizes to so-called YT bodies in the nucleus that contain active transcription sites. Tyrosine phosphorylation of YTHDC1 regulates its solubility in the nucleus and its effect on alternative splicing. Structural demonstration of YTHDC1 as an m⁶A reader raises a possible connection between m⁶A and alternative splicing [24, 25]. Among the YTH domain proteins, only YTHDC1 contains a selective binding pocket for the nucleotide preceding the m⁶A nucleotide [25]. Two pre-mRNA splicing factors SRSF3 and SRSF10 competitively bind to YTHDC1 [46]. It was proposed that YTHDC1 promotes exon inclusion by recruiting SRSF3 while blocking SRSF10 binding to target transcripts [46]. In this study, we find that YTHDC1 regulates mRNA splicing in oocytes. In addition, loss of YTHDC1 leads to formation of large novel cytoplasmic RNA-containing granules in the oocyte cytoplasm, which may contain aberrantly processed transcripts. Furthermore, the m⁶A-binding activity of YTHDC1 is required for rescue of alternative splicing defects in *Ythdc1*-deficient oocytes. Collectively, these *in vitro* and *in vivo* studies demonstrate the critical role of YTHDC1 in the regulation of alternative splicing, apparently in an m⁶A-dependent manner.

A number of studies show that m⁶A is a determinant of mRNA stability and turnover in the cytoplasm [23, 47, 76]. YTHDC1 facilitates nuclear export of m⁶A-containing mRNAs through its interaction with SRSF3 and thus regulates their cytoplasmic abundance [59]. YTHDC2 regulates the levels of m⁶A-containing transcripts in meiotic germ cells [32]. Binding by YTHDF2 causes redistribution of bound mRNAs to RNA degradation sites [23]. In addition, YTHDF2

regulates maternal mRNA clearance in both zebrafish and mouse [52, 53]. In contrast with the established role of m⁶A in mRNA turnover, the role of m⁶A in splicing has been a point of contention in the field. Some studies in ES cells conclude that m⁶A in nascent transcripts has a minor role in splicing, even though *Mettl3* inactivation in ES cells affects 3% of ~12,000 alternative cassette exons [47, 49]. It is possible that *Mettl3* inactivation may have more pronounced effect on splicing in differentiated cells. Indeed, *Mettl3* inactivation in male germ cells affects splicing [51]. The differentially spliced genes in *Ythdc1*-deficient oocytes significantly overlap with the differentially spliced genes in *Mettl3*-deficient testes (S8 Fig). Study of *Alkbh5*-deficient spermatogenic cells also supports a role of m⁶A in the regulation of splicing [74]. Therefore, the extent of effect on splicing by m⁶A most likely varies in different cell types and developmental stages.

Materials and methods

Ethics statement

Mice were maintained and used for experimentation according to the protocol approved by the Institutional Care and Use Committee of the University of Pennsylvania.

Generation of polyclonal antibodies

The GST-YTHDC1 (aa 3–109) fusion protein (S2A Fig) was expressed in *E. coli* using the pGEX4T-1 vector and affinity purified with glutathione Sepharose 4B (GE Healthcare). Rabbits were immunized with recombinant protein, yielding antisera UP2410 and UP2411 (Cocalico Biologicals Inc.). For western blotting and immunofluorescence, antibodies were affinity purified against the GST fusion protein.

Targeted inactivation of the *Ythdc1* gene

The *Ythdc1* targeting construct was designed to insert two tandem copies of *loxP*-flanked hygromycin phosphotransferase-thymidine kinase (HyTK) cassettes into *Ythdc1* intron 4, and a *loxP* site into intron 9 (S2B Fig). Genomic fragments were amplified from the *Ythdc1*-containing BAC clone RP24-567O8 by PCR with high-fidelity Taq DNA polymerase. The targeting construct was confirmed by sequencing. *Cla*I-linearized targeting construct was electroporated into V6.5 mouse embryonic stem (ES) cells, and ES cells were cultured in media containing 120 µg/ml hygromycin B. Of 368 hygromycin-resistant ES clones screened by long-range PCR, three clones were homologously targeted. Two positive clones (1A6 and 3D6) were expanded and electroporated with the *Cre*-expressing plasmid pOG231, followed by culture in media containing 2 µM ganciclovir. Ninety-six clones were screened for removal of the HyTK cassette and presence of *loxP* sites flanking *Ythdc1* exons 5–9 (S2B Fig), resulting in seven positive clones. Two (1A6H10 and 3D6G7) *Ythdc1*^{fl/+} ES clones were injected into blastocysts. The resulting chimeric mice transmitted the *Ythdc1* floxed allele through the germline.

Heterozygous (*Ythdc1*^{+/-}) animals were produced by mating *Ythdc1*^{fl/+} with *Actb*-*Cre* mice [60]. Mice with conditional deletion of *Ythdc1* were obtained from the intercrosses of *Ythdc1*^{fl/+} with *Ddx4*-*Cre* or *Zp3*-*Cre* mice [61, 62]. The resulting *Ythdc1*^{fl/+} *Cre* males were crossed with *Ythdc1*^{fl/fl} females, yielding *Ythdc1*^{fl/-} *Cre* mice with germline-specific inactivation. Offspring were genotyped by PCR of genomic DNA with the following primers: wild-type (396 bp) and *Ythdc1* floxed allele (473 bp), CTTCCAGCAGGAATGAGTGC and GGCAATAAATAGCCCCAAAA; *Ythdc1*⁻ (deletion) (426 bp), GATATCTTCTCTGATTCATGCG and GGCAATAAATAGCCCCAAAA; *Ddx4*-*Cre* (240 bp), CACGTGCAGCCGTTTAAGCCGCG

T and TTCCCATTCTAAACAACACCCTGAA; *Zp3-Cre* (220 bp), CCCAGATTCTGATCGT TGGT and CAGGTTCTTGCGAACCTCAT.

Collection and culture of mouse oocytes, eggs and embryos

Full-grown, germinal vesicle (GV)-intact oocytes, metaphase II (MII) eggs, fertilized eggs and preimplantation embryos were collected as previously described [77, 78]. GV oocytes were cultured in Chatot-Ziomek-Brinster (CZB) medium [79] containing 2.5 μ M milrinone (Sigma, St. Louis, MO, USA) to inhibit GV breakdown [80]; MII eggs were cultured in CZB medium and fertilized eggs/embryos cultured in KSOM [81].

GV oocytes were collected by poking of ovaries or enzymatic digestion. For enzymatic digestion, ovaries were dissected out and placed in Ca^{2+} - Mg^{2+} -free CZB medium containing 1 mg/ml collagenase (#LS004196, Worthington Biochemical Corp) and 0.2 mg/ml DNase I (Sigma #DN-25) in 35 mm petri dish. Each ovary was chopped into 4–5 pieces. Enzymatic digestion was carried out at 37°C for 40 min. Ovaries were pipetted up and down several times using a P1000 pipette to facilitate cell dissociation. Oocytes free of follicle cells were transferred and washed with three drops of CZB medium before further analysis.

Western blotting and immunocytochemistry

Equal numbers of GV oocytes, metaphase I (MI) eggs, MII eggs, fertilized eggs and embryos were lysed in 2xSDS loading buffer (Sigma). Lysates were separated by 10% SDS-PAGE gel electrophoresis and proteins transferred to PVDF membrane (Amersham). For western blot analysis of adult mouse tissues, tissue samples were collected from 8-week-old adult mice and 20 μ g of protein lysate per tissue analyzed per lane. The following antibodies/antisera were used for western blotting: rabbit anti-YTHDC1 affinity-purified antibody (this study); mouse anti-TUBB antibody (T4026, Sigma), mouse monoclonal ACTB (Clone AC-15, Sigma-Aldrich). Immuno-detection was performed using horseradish peroxidase-conjugated secondary antibodies and ECL prime reagents (Amersham) according to the manufacturer's instructions.

For immunofluorescence, oocyte, egg or embryo samples were fixed in 2.5% paraformaldehyde for 40 min at room temperature. Cells were permeabilized for 15 min in PBS containing 0.2% Triton X-100, blocked in PBS containing 0.2% IgG-free BSA and 0.01% Tween-20 for 30 min (blocking solution), and then incubated with the rabbit anti-YTHDC1 affinity-purified antibody for 1 h at room temperature. After four 15-min washes in blocking buffer, samples were incubated for 1 h with appropriate Cy5-conjugated secondary antibody (Jackson ImmunoResearch). After three additional 15-min washes in blocking buffer, the samples were mounted in Vectashield mounting solution with Sytox green (Vector Laboratories). Images were captured by a Leica TCS SP laser-scanning confocal microscope.

Immunofluorescence analysis in testis was performed as previously described [82]. Briefly, adult or neonatal testes were fixed in 4% formaldehyde for 3–4 h and processed for sectioning in a cryostat. Testicular sections were immunostained with anti-YTHDC1 and anti-SP10 antibodies [83]. FITC- or Texas red-conjugated secondary antibodies were used. Slides were mounted in VectaShield solution with DAPI (Vector Laboratories). Images were captured with an ORCA digital camera (Hamamatsu Photonics) on a Leica DM5500B microscope.

Whole-transcriptome RNA-seq analysis

Oocytes were collected from ovaries of 6-week-old wild-type or *Ythdc1*^{fl/fl}-*Ddx4*-Cre females by needle poking. Oocytes from *Ythdc1*^{fl/fl}-*Ddx4*-Cre females with gross abnormal morphology were excluded from studies. Total RNA was extracted from 25 oocytes per library using

PicoPure RNA isolation kit with on-column genomic DNA digestion according to the manufacturer's instruction (Thermo Fisher Scientific). As a normalization control, each sample was spiked in with 0.2 pg synthesized Renilla luciferase mRNA before extraction. RNA-seq libraries were constructed by using Ovation RNA-seq system V2 (NuGEN) followed by Ovation Ultralow Library system (DR Multiplex System, NuGEN). Reverse transcription of total RNA was primed with a pool of primers that hybridize either to the 5' portion of the poly(A) sequence or randomly across the transcript. Per genotype, three biological replicate libraries were constructed. RNA-seq libraries were pooled and sequenced by three 150-bp paired-end runs on mid-output flow cells on the NextSeq 550 system (Illumina) (S1 Table). RNA-seq data are available under the NCBI/SRA number: SRP116737.

Differential expression analysis

Oocyte RNA-seq data were mapped using the RNA-Seq aligner STAR. The STAR genome was generated using the mouse mm10 genome assembly (Genome Reference GRCm38). STAR was run with the parameter—clip3pAdapterSeq GATCGGAAGAGCACACGTCTGAACTC-CAGTCAC. The SAM files from STAR were converted to BAM format using samtools view, reads were sorted by name using samtools sort, and separate lanes were merged into one file using samtools merge [84]. The number of reads in each genomic feature was quantified with HTSeq using the intersection-strict overlap setting [85]. Differential abundance between *Ythdc1*^{fl/-} and *Ythdc1*-deficient oocytes was then analyzed using the R package DESeq2 on the HTSeq count files with default settings and an FDR cutoff of 0.01 [86].

Gene ontology (GO) analysis

Gene Ontology analysis was performed using the bioinformatics analysis resource database DAVID 6.8 [87]. Separate lists of differentially expressed up-regulated and down-regulated genes (all, FDR < 0.01, Fold change ≥ 2 , and mean expression ≥ 100) were uploaded, with the Genbank_accession identifier selected and mus_musculus as the specified organism. A custom background list was supplied consisting of all genes with at least one read observed in any genotype or replicate in our RNA-seq libraries.

Bioinformatic analysis of local splicing variants (LSVs) by MAJIQ

Analysis of units of LSVs between *Ythdc1*^{fl/-} and *Ythdc1*-deficient oocytes was performed using the MAJIQ software package [63]. MAJIQ v0.9.2 was run using the GRCm38 mm10 reference genome. Default settings were used for quantifying LSVs in the oocyte RNA-seq data and for the Δ PSI analysis. Please note that MAJIQ was not designed to identify alternative polyadenylation from RNA-seq data [63].

Bioinformatic analysis of alternative polyadenylation by ROAR

Alternative polyadenylation (APA) analysis was performed with the ROAR Bioconductor package in R [67]. The package's general workflow was followed. GV oocyte RNA-seq reads were mapped to the mm9 (NCBI37) genome using the RNA STAR aligner. ROAR was run using an annotation database of polyadenylation sites from the PolyADB version 2 [88]. The ratio of shorter to longer isoforms referred to as m/M ratio was computed for each sample using the counts of mapped reads and the lengths of the transcript's PRE and POST portions as defined using a multiple APA annotation file. The ratio of the $m/M_{(WT)}$ to the $m/M_{(KO)}$ yielded the ratio of a ratio (ROAR) values, which were used to identify shifts in polyadenylation site usage. 3' UTR lengthening or shortening was called when a Fisher test for all sample

pairings returned nominal p -values < 0.05 . We analyzed the RNA-seq data from the SRSF3 and SRSF7 knockdown experiments by Muller-McNicoll *et al.* [73] using the ROAR algorithm and reached the same conclusions on opposing changes on 3' UTR length, validating the ROAR algorithm.

Validation of differentially expressed genes by quantitative real-time PCR

Oocytes were collected from 6-week-old wild-type or *Ythdc1*^{fl/-} *Ddx4*-Cre or *Ythdc1*^{fl/-} *Zp3*-Cre females by needle poking of ovaries. Total RNA was extracted from oocytes using the PicoPure RNA Isolation Kit with on-column genomic DNA digestion (Thermo Fisher Scientific) and reverse transcribed by Superscript II reverse transcriptase (Invitrogen) using random hexamers. The resulting cDNA was quantified by real-time PCR on an ABI Prism 7000 thermocycler (Applied Biosystems) using Power SYBR Green Master Mix (Thermo Fisher Scientific). The following gene transcripts were tested: *Psat1*, *Grhl3*, *Cnnm1*, *Nupr*, *Zfp711*, *Lrp1b*, *Rgn*, *Trps1*, *Tnip3*, *Piwil1* (Oligonucleotide primer sequences in [S5 Table](#)). PCR parameters: 95°C, 15 sec; 60°C, 60 sec; 40 cycles. Each sample was analyzed in duplicates. Quantification was normalized to the endogenous *Actb* using the comparative Ct method (ABI Prism 7700 Sequence Detection System, Applied Biosystems).

Validation of local splicing variants and APA

For validation of local splicing variants, each PCR assay was optimized individually ([S5 Table](#)). The PCR cycles varied for each LSV, depending on transcript abundance. For APA validation, two pairs of PCR primers were designed: PRE and POST (before and after the polyadenylation site) ([S5 Table](#)). All assays used an amount of cDNA equivalent to one oocyte per PCR reaction. RT-PCR band quantification was performed using ImageJ.

Histological analysis

Testes and ovaries were prepared for histological analysis by fixation in Bouin's solution (Sigma Aldrich), followed by serial dehydration and paraffin infiltration and embedding. Serial sections were cut at 8 μ m thickness, adhered to glass slides, and dried overnight. Slides were de-paraffinized with xylene and re-hydrated. Slides were then stained with hematoxylin, rinsed, and exposed to 0.1 M ammonia before staining with eosin. The slides were then dehydrated and mounted with Permount mounting media (Fisher Scientific). Images were taken on a DM5500B microscopy platform with a DFC450 camera (Leica Microsystems).

DNA constructs and mutagenesis

Wild-type mouse *Ythdc1* coding region was amplified from bulk mouse testis cDNA samples by PCR. The double mutation (W377A, W428A) was introduced by PCR-based mutagenesis by mutating codons 377 (TGG) 428 (TGG) to 377 (GCG) 428 (GCG), resulting in W377A W428A amino acid changes. The entire coding region was cloned into the pcDNA3.1 vector for in vitro transcription.

In vitro transcription

Plasmids pcDNA3.1-wt-*Ythdc1* and pcDNA3.1-*Ythdc1*-W377A W428A were verified by sequencing and linearized before in vitro transcription. Capped mRNAs were made by in vitro transcription with T7 mScript mRNA production System (CellSCRIPT) according to the manufacturer's instructions. Following in vitro transcription, template DNAs were digested by adding RNase-free DNase, and synthesized mRNA was purified by MEGAclean kit (Ambion).

A single mRNA band of the expected size was observed for each RNA sample on a 1% formaldehyde denaturing gel. Synthesized RNA was stored in aliquots at -80°C .

Oocyte microinjection and LSV rescue assay

GV oocytes were collected from postnatal day 12 *Ythdc1*-deficient ovaries by enzymatic digestion (collagenase). Oocytes were microinjected with approximately 5 pl of wild-type or mutant *Ythdc1* mRNA in water as previously described [89]. PND12 wild-type oocytes were mock injected with water as controls. Following microinjection, oocytes were returned to CZB medium with 2.5 μM milrinone and cultured overnight, followed by RNA extraction and reverse transcription. For LSV rescue experiments, each PCR assay was performed using an amount of cDNA equivalent to 0.5 oocyte. PCR bands were quantified using the Image J software. The rescue experiments were performed two times.

Transfection and co-immunoprecipitation

The FLAG-YTHDC1 expression construct was made by cloning the full-length mouse *Ythdc1* coding sequence into a pcDNA6 vector containing a previously inserted 3xFLAG sequence 5' of the cloning site. V5 tagged constructs for *Srsf7*, *Cstf1*, *Cstf2*, *Cpsf6*, and *Nudt21* were all produced by subcloning RT-PCR products amplified from bulk mouse testis cDNAs using the pcDNA 3.1/V5-His TOPO TA Expression Kit (Invitrogen, K4800). *Srsf3* cDNA was cloned into a pcDNA6 vector containing a Myc tag 5' of the cloning site to express Myc-SRSF3. The HEK 293T cells were cultured in Dulbecco's Modified Eagle Medium (DMEM) supplemented with 10% fetal bovine serum (FBS), 1% penicillin/streptomycin, and 1% L-glutamine in a 37°C humidified incubator at 5% CO_2 . Cells were co-transfected using Lipofectamine 2000 (Invitrogen) and cultured in Opti-mem media for 36 h. Transfected cells were harvested with RIPA buffer (10 mM Tris-HCl, pH 8, 1 mM EDTA, 0.5 mM EGTA, 1% Triton X-100, 0.1% SDS, 140 mM NaCl, 0.1% sodium deoxycholate) supplemented with 1 mM phenylmethylsulfonyl fluoride (PMSF). Cells were lysed by Dounce homogenization and solubilized by rocking at 4°C for 30 min. Following centrifugation at 16,100 x g for 25 min, lysate supernatants were incubated with 1 mg/ml RNase A at room temperature for 30 min. Lysates were cleared by centrifugation at 16,100 x g for 20 min and incubated with Protein G agarose beads (Invitrogen, 15920010) for 1 h. After pre-clearing, either anti-FLAG (F-3165, Sigma), anti-V5 (R96025, ThermoFisher), or anti-Myc (631206, Clontech) was incubated with cell lysates rotating overnight at 4°C . Equilibrated Protein G agarose beads were added to the lysates and incubated for 1 h. Immunoprecipitated protein complexes were washed three times with RIPA buffer supplemented with PMSF. Beads and respective input lysates were boiled with 2x SDS sample buffer for 5 min prior to SDS-PAGE and immunoblotting to nitrocellulose membranes.

Supporting information

S1 Fig. Nuclear localization of YTHDC1 in transcriptionally active male germ cells: Spermatogonia, spermatocytes, and round spermatids. (A) Frozen testicular sections from 8-week-old wild-type males were immunostained with anti-YTHDC1 and anti-SP10 antibodies. SP10 (also called ACRV1) is a component of the acrosome and thus used for seminiferous tubule staging [83]. DNA was stained with DAPI. Tubules at stages V, IX, and XII are shown. Scale bar, 50 μm . (B) Summary of YTHDC1 protein expression during spermatogenesis. The diagram of spermatogenesis was re-drawn as previously illustrated [90]. Expression of YTHDC1 protein is shown in green. Stages (I–XII) of spermatogenesis are shown. Spg, spermatogonia; PL, pre-leptotene; L, leptotene; Z, zygotene; P, pachytene; D, diplotene; M,

metaphase spermatocyte; RS, round spermatid; and ES, elongating spermatid. (TIF)

S2 Fig. Conditional inactivation of the *Ythdc1* gene. (A) The only known motif in YTHDC1 is the YTH domain. The antibody was raised against the N-terminal region encompassing amino acids (aa) 3–109. Mouse YTHDC1 protein reference sequence: NP_808348.2. (B) Diagram of wild-type and targeted *Ythdc1* alleles. Mouse *Ythdc1* maps to Chromosome 5 and consists of 17 exons. Targeted deletion of exons 5–9 (aa 296–452) results in a frame shift in the transcribed mRNA and removes the YTH domain. (C) Ubiquitous inactivation of *Ythdc1* is embryonic lethal. Timed matings of *Ythdc1*^{fl/-} mice were set up, and embryos/pups collected and genotyped at the time points shown. Numbers in brackets marked with asterisks indicate the number of resorptions found.

(TIF)

S3 Fig. Absence of YTHDC1 protein in male germ cells from neonatal *Ythdc1*^{fl/-} *Ddx4*-Cre testes. Frozen testicular sections from neonatal wild-type and *Ythdc1*^{fl/-} *Ddx4*-Cre males were immunostained with anti-YTHDC1 antibody. Nuclear DNA was stained with DAPI. Gonocytes (also called prospermatogonia) are indicated by white arrowheads. YTHDC1 is nuclear in wild-type gonocytes but absent in *Ythdc1*^{fl/-} *Ddx4*-Cre gonocytes. Scale bar, 25 μm.

(TIF)

S4 Fig. Absence of YTHDC1 protein in *Ythdc1*^{fl/-} *Ddx4*-Cre oocytes. Oocytes were collected from 6-week-old mice. (A) Western blot analysis of oocytes from wild-type and *Ythdc1* cKO (*Ythdc1*^{fl/-} *Ddx4*-Cre) females. TUBB (β-tubulin) served as a loading control. (B) YTHDC1 immunostaining of wild-type and *Ythdc1* cKO (*Ythdc1*^{fl/-} *Ddx4*-Cre) oocytes. Nuclei/nuclear DNA and cytoplasmic RNA granules are marked by arrowheads (blue) and arrows (white), respectively. Sytox green stains both DNA and RNA. Please note that all the Sytox green signals in the wild type oocyte were from nuclear DNA staining.

(TIF)

S5 Fig. Dysregulated transcriptome in *Ythdc1*-deficient oocytes. (A) Scatter plot of transcript profiling between wild-type and *Ythdc1*^{fl/-} *Ddx4*-Cre oocytes from 6-week-old females. FDR cutoff: 0.01. The list of differentially expressed transcripts is shown in [S2 Table](#). (B) Validation of 10 differentially expressed genes by real-time PCR. Real-time PCR was performed in duplicates. The average and range are shown. (C) GO term enrichment in up-regulated and down-regulated genes in *Ythdc1*-deficient oocytes. Differentially expressed genes with FDR < 0.01, Fold change ≥ 2, and mean expression ≥ 100 were included in the GO analysis.

(TIF)

S6 Fig. GO term enrichment in MAJIQ-called genes with LSVs between wild-type and *Ythdc1*-deficient oocytes.

(TIF)

S7 Fig. PCR validation of LSVs affecting internal exons in *Ythdc1*-deficient oocytes.

Oocytes were collected from 6-week-old *Ythdc1*^{fl/+} and *Ythdc1*^{fl/-} *Zp3*-Cre females. Exons are represented as rectangles but not in scale. Skipped or retained exons are shown in red. Triangles denote the positions of PCR primers.

(TIF)

S8 Fig. Significant overlap of differentially spliced genes in *Ythdc1*-deficient oocytes and *Mettl3* knockout testes. The RNA-seq data from control and *Mettl3* knockout postnatal day 12 testes from the previous Xu *et al* study [51] were re-analyzed by MAJIQ. Statistics was

performed by hypergeometric enrichment tests.
(TIF)

S1 Table. Sequence reads of six oocyte RNA-seq libraries (3 wild-type and 3 *Ythdc1* cKO).
(XLSX)

S2 Table. Differentially expressed genes between wild-type and *Ythdc1*-deficient oocytes from 6-week-old females. FDR cutoff of 0.01 was used.
(XLSX)

S3 Table. MAJIQ-identified local splicing variants (LSVs) between wild-type and *Ythdc1*-deficient oocytes from 6-week-old females.
(XLSX)

S4 Table. ROAR output of alternative polyadenylation events between wild-type and *Ythdc1*-deficient oocytes.
(XLSX)

S5 Table. Oligos for qPCR, LSV validation, and APA validation.
(XLSX)

Acknowledgments

We thank Ana Misic and Daniel Beiting at CHMI for help with next-gen sequencing, Prabhakara Reddi for anti-SP10 (ACRV1) antibodies, and Sigrid Eckardt for help with manuscript preparation.

Author Contributions

Conceptualization: Seth D. Kasowitz, Jun Ma, Brian D. Gregory, Richard M. Schultz, P. Jeremy Wang.

Data curation: Seth D. Kasowitz, Jun Ma, Stephen J. Anderson.

Formal analysis: Seth D. Kasowitz, Jun Ma, Stephen J. Anderson, Brian D. Gregory, Richard M. Schultz, P. Jeremy Wang.

Funding acquisition: Brian D. Gregory, Richard M. Schultz, P. Jeremy Wang.

Investigation: Seth D. Kasowitz, Jun Ma, Stephen J. Anderson, N. Adrian Leu, Yang Xu, P. Jeremy Wang.

Methodology: Seth D. Kasowitz, Jun Ma, Stephen J. Anderson, N. Adrian Leu, Yang Xu, P. Jeremy Wang.

Resources: N. Adrian Leu, Brian D. Gregory, P. Jeremy Wang.

Supervision: Brian D. Gregory, Richard M. Schultz, P. Jeremy Wang.

Validation: P. Jeremy Wang.

Writing – original draft: Seth D. Kasowitz, Jun Ma, Stephen J. Anderson, P. Jeremy Wang.

Writing – review & editing: Seth D. Kasowitz, Jun Ma, Stephen J. Anderson, N. Adrian Leu, Yang Xu, Brian D. Gregory, Richard M. Schultz, P. Jeremy Wang.

References

1. Machnicka MA, Milanowska K, Osman Oglou O, Purta E, Kurkowska M, et al. (2013) MODOMICS: A database of RNA modification pathways—2013 update. *Nucleic Acids Res* 41: D262–7. <https://doi.org/10.1093/nar/gks1007> PMID: 23118484
2. Meyer KD, Jaffrey SR. (2014) The dynamic epitranscriptome: N6-methyladenosine and gene expression control. *Nat Rev Mol Cell Biol* 15: 313–326. <https://doi.org/10.1038/nrm3785> PMID: 24713629
3. Yue Y, Liu J, He C. (2015) RNA N6-methyladenosine methylation in post-transcriptional gene expression regulation. *Genes Dev* 29: 1343–1355. <https://doi.org/10.1101/gad.262766.115> PMID: 26159994
4. Liu N, Pan T. (2016) N6-methyladenosine-encoded epitranscriptomics. *Nat Struct Mol Biol* 23: 98–102. <https://doi.org/10.1038/nsmb.3162> PMID: 26840897
5. Meyer KD, Saletore Y, Zumbo P, Elemento O, Mason CE, et al. (2012) Comprehensive analysis of mRNA methylation reveals enrichment in 3' UTRs and near stop codons. *Cell* 149: 1635–1646. <https://doi.org/10.1016/j.cell.2012.05.003> PMID: 22608085
6. Dominissini D, Moshitch-Moshkovitz S, Schwartz S, Salmon-Divon M, Ungar L, et al. (2012) Topology of the human and mouse m6A RNA methylomes revealed by m6A-seq. *Nature* 485: 201–206. <https://doi.org/10.1038/nature11112> PMID: 22575960
7. Batista PJ, Molinie B, Wang J, Qu K, Zhang J, et al. (2014) m(6)A RNA modification controls cell fate transition in mammalian embryonic stem cells. *Cell Stem Cell* 15: 707–719. <https://doi.org/10.1016/j.stem.2014.09.019> PMID: 25456834
8. Schwartz S, Mumbach MR, Jovanovic M, Wang T, Maciag K, et al. (2014) Perturbation of m6A writers reveals two distinct classes of mRNA methylation at internal and 5' sites. *Cell Rep* 8: 284–296. <https://doi.org/10.1016/j.celrep.2014.05.048> PMID: 24981863
9. Ke S, Alemu EA, Mertens C, Gantman EC, Fak JJ, et al. (2015) A majority of m6A residues are in the last exons, allowing the potential for 3' UTR regulation. *Genes Dev* 29: 2037–2053. <https://doi.org/10.1101/gad.269415.115> PMID: 26404942
10. Patil DP, Chen CK, Pickering BF, Chow A, Jackson C, et al. (2016) m6A RNA methylation promotes XIST-mediated transcriptional repression. *Nature* 537: 369–373. <https://doi.org/10.1038/nature19342> PMID: 27602518
11. Shimba S, Bokar JA, Rottman F, Reddy R. (1995) Accurate and efficient N-6-adenosine methylation in spliceosomal U6 small nuclear RNA by HeLa cell extract in vitro. *Nucleic Acids Res* 23: 2421–2426. PMID: 7630720
12. Piekna-Przybylska D, Decatur WA, Fournier MJ. (2008) The 3D rRNA modification maps database: With interactive tools for ribosome analysis. *Nucleic Acids Res* 36: D178–83. <https://doi.org/10.1093/nar/gkm855> PMID: 17947322
13. Clancy MJ, Shambaugh ME, Timpte CS, Bokar JA. (2002) Induction of sporulation in *Saccharomyces cerevisiae* leads to the formation of N6-methyladenosine in mRNA: A potential mechanism for the activity of the IME4 gene. *Nucleic Acids Res* 30: 4509–4518. PMID: 12384598
14. Schwartz S, Agarwala SD, Mumbach MR, Jovanovic M, Mertins P, et al. (2013) High-resolution mapping reveals a conserved, widespread, dynamic mRNA methylation program in yeast meiosis. *Cell* 155: 1409–1421. <https://doi.org/10.1016/j.cell.2013.10.047> PMID: 24269006
15. Haussmann IU, Bodi Z, Sanchez-Moran E, Mongan NP, Archer N, et al. (2016) m6A potentiates *sxl* alternative pre-mRNA splicing for robust *Drosophila* sex determination. *Nature* 540: 301–304. <https://doi.org/10.1038/nature20577> PMID: 27919081
16. Lence T, Akhtar J, Bayer M, Schmid K, Spindler L, et al. (2016) m6A modulates neuronal functions and sex determination in *Drosophila*. *Nature* 540: 242–247. <https://doi.org/10.1038/nature20568> PMID: 27919077
17. Luo GZ, MacQueen A, Zheng G, Duan H, Dore LC, et al. (2014) Unique features of the m6A methylome in *Arabidopsis thaliana*. *Nat Commun* 5: 5630. <https://doi.org/10.1038/ncomms6630> PMID: 25430002
18. Bokar JA, Shambaugh ME, Polayes D, Matera AG, Rottman FM. (1997) Purification and cDNA cloning of the AdoMet-binding subunit of the human mRNA (N6-adenosine)-methyltransferase. *Rna* 3: 1233–1247. PMID: 9409616
19. Liu J, Yue Y, Han D, Wang X, Fu Y, et al. (2014) A METTL3-METTL14 complex mediates mammalian nuclear RNA N6-adenosine methylation. *Nat Chem Biol* 10: 93–95. <https://doi.org/10.1038/nchembio.1432> PMID: 24316715
20. Ping XL, Sun BF, Wang L, Xiao W, Yang X, et al. (2014) Mammalian WTAP is a regulatory subunit of the RNA N6-methyladenosine methyltransferase. *Cell Res* 24: 177–189. <https://doi.org/10.1038/cr.2014.3> PMID: 24407421

21. Jia G, Fu Y, Zhao X, Dai Q, Zheng G, et al. (2011) N6-methyladenosine in nuclear RNA is a major substrate of the obesity-associated FTO. *Nat Chem Biol* 7: 885–887. <https://doi.org/10.1038/nchembio.687> PMID: 22002720
22. Zheng G, Dahl JA, Niu Y, Fedorcsak P, Huang CM, et al. (2013) ALKBH5 is a mammalian RNA demethylase that impacts RNA metabolism and mouse fertility. *Mol Cell* 49: 18–29. <https://doi.org/10.1016/j.molcel.2012.10.015> PMID: 23177736
23. Wang X, Lu Z, Gomez A, Hon GC, Yue Y, et al. (2014) N6-methyladenosine-dependent regulation of messenger RNA stability. *Nature* 505: 117–120. <https://doi.org/10.1038/nature12730> PMID: 24284625
24. Xu C, Wang X, Liu K, Roundtree IA, Tempel W, et al. (2014) Structural basis for selective binding of m6A RNA by the YTHDC1 YTH domain. *Nat Chem Biol* 10: 927–929. <https://doi.org/10.1038/nchembio.1654> PMID: 25242552
25. Xu C, Liu K, Ahmed H, Loppnau P, Schapira M, et al. (2015) Structural basis for the discriminative recognition of N6-methyladenosine RNA by the human YT521-B homology domain family of proteins. *J Biol Chem* 290: 24902–24913. <https://doi.org/10.1074/jbc.M115.680389> PMID: 26318451
26. Hsu PJ, Zhu Y, Ma H, Guo Y, Shi X, et al. (2017) Ythdc2 is an N(6)-methyladenosine binding protein that regulates mammalian spermatogenesis. *Cell Res* 27: 1115–1127. <https://doi.org/10.1038/cr.2017.99> PMID: 28809393
27. Hartmann AM, Nayler O, Schwaiger FW, Obermeier A, Stamm S. (1999) The interaction and colocalization of Sam68 with the splicing-associated factor YT521-B in nuclear dots is regulated by the src family kinase p59(fyn). *Mol Biol Cell* 10: 3909–3926. PMID: 10564280
28. Nayler O, Hartmann AM, Stamm S. (2000) The ER repeat protein YT521-B localizes to a novel subnuclear compartment. *J Cell Biol* 150: 949–962. PMID: 10973987
29. Abby E, Tourpin S, Ribeiro J, Daniel K, Messiaen S, et al. (2016) Implementation of meiosis prophase I programme requires a conserved retinoid-independent stabilizer of meiotic transcripts. *Nat Commun* 7: 10324. <https://doi.org/10.1038/ncomms10324> PMID: 26742488
30. Soh YQS, Mikedis MM, Kojima M, Godfrey AK, de Rooij DG, et al. (2017) Meioc maintains an extended meiotic prophase I in mice. *PLoS Genet* 13: e1006704. <https://doi.org/10.1371/journal.pgen.1006704> PMID: 28380054
31. Bailey AS, Batista PJ, Gold RS, Chen YG, de Rooij DG, et al. (2017) The conserved RNA helicase YTHDC2 regulates the transition from proliferation to differentiation in the germline. *Elife* 6: <https://doi.org/10.7554/eLife.26116> PMID: 29087293
32. Wojtas MN, Pandey RR, Mendel M, Homolka D, Sachidanandam R, et al. (2017) Regulation of m(6)A transcripts by the 3'→5' RNA helicase YTHDC2 is essential for a successful meiotic program in the mammalian germline. *Mol Cell* 68: 374–387. <https://doi.org/10.1016/j.molcel.2017.09.021> PMID: 29033321
33. Jain D, Puno MR, Meydan C, Lailier N, Mason CE, et al. (2018) Ketu mutant mice uncover an essential meiotic function for the ancient RNA helicase YTHDC2. *Elife* 7: <https://doi.org/10.7554/eLife.30919> PMID: 29360036
34. Schibler U, Kelley DE, Perry RP. (1977) Comparison of methylated sequences in messenger RNA and heterogeneous nuclear RNA from mouse L cells. *J Mol Biol* 115: 695–714. PMID: 592376
35. Zhang Z, Theler D, Kaminska KH, Hiller M, de la Grange P, et al. (2010) The YTH domain is a novel RNA binding domain. *J Biol Chem* 285: 14701–14710. <https://doi.org/10.1074/jbc.M110.104711> PMID: 20167602
36. Huang H, Weng H, Sun W, Qin X, Shi H, et al. (2018) Recognition of RNA N(6)-methyladenosine by IGF2BP proteins enhances mRNA stability and translation. *Nat Cell Biol* 20: 285–295. <https://doi.org/10.1038/s41556-018-0045-z> PMID: 29476152
37. Edupuganti RR, Geiger S, Lindeboom RGH, Shi H, Hsu PJ, et al. (2017) N(6)-methyladenosine (m(6)A) recruits and repels proteins to regulate mRNA homeostasis. *Nat Struct Mol Biol* 24: 870–878. <https://doi.org/10.1038/nsmb.3462> PMID: 28869609
38. Meyer KD, Patil DP, Zhou J, Zinoviev A, Skabkin MA, et al. (2015) 5' UTR m(6)A promotes cap-independent translation. *Cell* 163: 999–1010. <https://doi.org/10.1016/j.cell.2015.10.012> PMID: 26593424
39. Alarcon CR, Goodarzi H, Lee H, Liu X, Tavazoie S, et al. (2015) HNRNPA2B1 is a mediator of m(6)A-dependent nuclear RNA processing events. *Cell* 162: 1299–1308. <https://doi.org/10.1016/j.cell.2015.08.011> PMID: 26321680
40. Wu B, Su S, Patil DP, Liu H, Gan J, et al. (2018) Molecular basis for the specific and multivalent recognitions of RNA substrates by human hnRNP A2/B1. *Nat Commun* 9: 420-017-02770-z.
41. Liu N, Dai Q, Zheng G, He C, Parisien M, et al. (2015) N(6)-methyladenosine-dependent RNA structural switches regulate RNA-protein interactions. *Nature* 518: 560–564. <https://doi.org/10.1038/nature14234> PMID: 25719671

42. Liu N, Zhou KI, Parisien M, Dai Q, Diatchenko L, et al. (2017) N6-methyladenosine alters RNA structure to regulate binding of a low-complexity protein. *Nucleic Acids Res* 45: 6051–6063. <https://doi.org/10.1093/nar/gkx141> PMID: 28334903
43. Mauer J, Luo X, Blanjoie A, Jiao X, Grozhik AV, et al. (2017) Reversible methylation of m6Am in the 5' cap controls mRNA stability. *Nature* 541: 371–375. <https://doi.org/10.1038/nature21022> PMID: 28002401
44. Meyer KD, Patil DP, Zhou J, Zinoviev A, Skabkin MA, et al. (2015) 5' UTR m(6)A promotes cap-independent translation. *Cell* 163: 999–1010. <https://doi.org/10.1016/j.cell.2015.10.012> PMID: 26593424
45. Wang X, Zhao BS, Roundtree IA, Lu Z, Han D, et al. (2015) N(6)-methyladenosine modulates messenger RNA translation efficiency. *Cell* 161: 1388–1399. <https://doi.org/10.1016/j.cell.2015.05.014> PMID: 26046440
46. Xiao W, Adhikari S, Dahal U, Chen YS, Hao YJ, et al. (2016) Nuclear m(6)A reader YTHDC1 regulates mRNA splicing. *Mol Cell* 61: 507–519. <https://doi.org/10.1016/j.molcel.2016.01.012> PMID: 26876937
47. Ke S, Pandya-Jones A, Saito Y, Fak JJ, Vagbo CB, et al. (2017) m6A mRNA modifications are deposited in nascent pre-mRNA and are not required for splicing but do specify cytoplasmic turnover. *Genes Dev* 31: 990–1006. <https://doi.org/10.1101/gad.301036.117> PMID: 28637692
48. Hongay CF, Orr-Weaver TL. (2011) Drosophila inducer of MEiosis 4 (IME4) is required for notch signaling during oogenesis. *Proc Natl Acad Sci U S A* 108: 14855–14860. <https://doi.org/10.1073/pnas.1111577108> PMID: 21873203
49. Geula S, Moshitch-Moshkovitz S, Dominissini D, Mansour AA, Kol N, et al. (2015) Stem cells. m6A mRNA methylation facilitates resolution of naive pluripotency toward differentiation. *Science* 347: 1002–1006. <https://doi.org/10.1126/science.1261417> PMID: 25569111
50. Lin Z, Hsu PJ, Xing X, Fang J, Lu Z, et al. (2017) Mettl3-/Mettl14-mediated mRNA N(6)-methyladenosine modulates murine spermatogenesis. *Cell Res* 27: 1216–1230. <https://doi.org/10.1038/cr.2017.117> PMID: 28914256
51. Xu K, Yang Y, Feng GH, Sun BF, Chen JQ, et al. (2017) Mettl3-mediated m(6)A regulates spermatogonial differentiation and meiosis initiation. *Cell Res* 27: 1100–1114. <https://doi.org/10.1038/cr.2017.100> PMID: 28809392
52. Zhao BS, Wang X, Beadell AV, Lu Z, Shi H, et al. (2017) m6A-dependent maternal mRNA clearance facilitates zebrafish maternal-to-zygotic transition. *Nature* 542: 475–478. <https://doi.org/10.1038/nature21355> PMID: 28192787
53. Ivanova I, Much C, Di Giacomo M, Azzi C, Morgan M, et al. (2017) The RNA m(6)A reader YTHDF2 is essential for the post-transcriptional regulation of the maternal transcriptome and oocyte competence. *Mol Cell* 67: 1059–1067.e4. <https://doi.org/10.1016/j.molcel.2017.08.003> PMID: 28867294
54. Fustin JM, Doi M, Yamaguchi Y, Hida H, Nishimura S, et al. (2013) RNA-methylation-dependent RNA processing controls the speed of the circadian clock. *Cell* 155: 793–806. <https://doi.org/10.1016/j.cell.2013.10.026> PMID: 24209618
55. Wang Y, Li Y, Toth JI, Petroski MD, Zhang Z, et al. (2014) N6-methyladenosine modification destabilizes developmental regulators in embryonic stem cells. *Nat Cell Biol* 16: 191–198. <https://doi.org/10.1038/ncb2902> PMID: 24394384
56. Chen T, Hao YJ, Zhang Y, Li MM, Wang M, et al. (2015) m(6)A RNA methylation is regulated by microRNAs and promotes reprogramming to pluripotency. *Cell Stem Cell* 16: 289–301. <https://doi.org/10.1016/j.stem.2015.01.016> PMID: 25683224
57. Luo M, Yang F, Leu NA, Landaiche J, Handel MA, et al. (2013) MEIOB exhibits single-stranded DNA-binding and exonuclease activities and is essential for meiotic recombination. *Nat Commun* 4: 2788. <https://doi.org/10.1038/ncomms3788> PMID: 24240703
58. Rafalska I, Zhang Z, Benderska N, Wolff H, Hartmann AM, et al. (2004) The intranuclear localization and function of YT521-B is regulated by tyrosine phosphorylation. *Hum Mol Genet* 13: 1535–1549. <https://doi.org/10.1093/hmg/ddh167> PMID: 15175272
59. Roundtree IA, Luo GZ, Zhang Z, Wang X, Zhou T, et al. (2017) YTHDC1 mediates nuclear export of N(6)-methyladenosine methylated mRNAs. *Elife* 6: <https://doi.org/10.7554/eLife.31311> PMID: 28984244
60. Lewandoski M, Meyers EN, Martin GR. (1997) Analysis of Fgf8 gene function in vertebrate development. *Cold Spring Harb Symp Quant Biol* 62: 159–168. PMID: 9598348
61. Gallardo T, Shirley L, John GB, Castrillon DH. (2007) Generation of a germ cell-specific mouse transgenic cre line, vasa-cre. *Genesis* 45: 413–417. <https://doi.org/10.1002/dvg.20310> PMID: 17551945
62. de Vries WN, Binns LT, Fancher KS, Dean J, Moore R, et al. (2000) Expression of cre recombinase in mouse oocytes: A means to study maternal effect genes. *Genesis* 26: 110–112. PMID: 10686600

63. Vaquero-Garcia J, Barrera A, Gazzara MR, Gonzalez-Vallinas J, Lahens NF, et al. (2016) A new view of transcriptome complexity and regulation through the lens of local splicing variations. *Elife* 5: e11752. <https://doi.org/10.7554/eLife.11752> PMID: 26829591
64. Ji Z, Lee JY, Pan Z, Jiang B, Tian B. (2009) Progressive lengthening of 3' untranslated regions of mRNAs by alternative polyadenylation during mouse embryonic development. *Proc Natl Acad Sci U S A* 106: 7028–7033. <https://doi.org/10.1073/pnas.0900028106> PMID: 19372383
65. Zhang Y, Tang C, Yu T, Zhang R, Zheng H, et al. (2017) MicroRNAs control mRNA fate by compartmentalization based on 3' UTR length in male germ cells. *Genome Biol* 18: 105 <https://doi.org/10.1186/s13059-017-1243-x> PMID: 28615029.
66. Miura P, Shenker S, Andreu-Agullo C, Westholm JO, Lai EC. (2013) Widespread and extensive lengthening of 3' UTRs in the mammalian brain. *Genome Res* 23: 812–825. <https://doi.org/10.1101/gr.146886.112> PMID: 23520388
67. Grassi E, Mariella E, Lembo A, Molineris I, Provero P. (2016) Roar: Detecting alternative polyadenylation with standard mRNA sequencing libraries. *BMC Bioinformatics* 17: 423. <https://doi.org/10.1186/s12859-016-1254-8> PMID: 27756200
68. Elkon R, Ugalde AP, Agami R. (2013) Alternative cleavage and polyadenylation: Extent, regulation and function. *Nat Rev Genet* 14: 496–506. <https://doi.org/10.1038/nrg3482> PMID: 23774734
69. Tian B, Manley JL. (2017) Alternative polyadenylation of mRNA precursors. *Nat Rev Mol Cell Biol* 18: 18–30. <https://doi.org/10.1038/nrm.2016.116> PMID: 27677860
70. Martin G, Gruber AR, Keller W, Zavolan M. (2012) Genome-wide analysis of pre-mRNA 3' end processing reveals a decisive role of human cleavage factor I in the regulation of 3' UTR length. *Cell Rep* 1: 753–763. <https://doi.org/10.1016/j.celrep.2012.05.003> PMID: 22813749
71. Li W, You B, Hoque M, Zheng D, Luo W, et al. (2015) Systematic profiling of poly(A)+ transcripts modulated by core 3' end processing and splicing factors reveals regulatory rules of alternative cleavage and polyadenylation. *PLoS Genet* 11: e1005166. <https://doi.org/10.1371/journal.pgen.1005166> PMID: 25906188
72. Sasado T, Kondoh H, Furutani-Seiki M, Naruse K. (2017) Mutation in cpsf6/CFIm68 (cleavage and polyadenylation specificity factor subunit 6) causes short 3'UTRs and disturbs gene expression in developing embryos, as revealed by an analysis of primordial germ cell migration using the medaka mutant naruto. *PLoS One* 12: e0172467. <https://doi.org/10.1371/journal.pone.0172467> PMID: 28253363
73. Muller-McNicol M, Botti V, de Jesus Domingues AM, Brandl H, Schwich OD, et al. (2016) SR proteins are NXF1 adaptors that link alternative RNA processing to mRNA export. *Genes Dev* 30: 553–566. <https://doi.org/10.1101/gad.276477.115> PMID: 26944680
74. Tang C, Klukovich R, Peng H, Wang Z, Yu T, et al. (2018) ALKBH5-dependent m6A demethylation controls splicing and stability of long 3'-UTR mRNAs in male germ cells. *Proc Natl Acad Sci U S A* 115: E325–E333. <https://doi.org/10.1073/pnas.1717794115> PMID: 29279410
75. Dong J, Albertini DF, Nishimori K, Kumar TR, Lu N, et al. (1996) Growth differentiation factor-9 is required during early ovarian folliculogenesis. *Nature* 383: 531–535. <https://doi.org/10.1038/383531a0> PMID: 8849725
76. Camper SA, Albers RJ, Coward JK, Rottman FM. (1984) Effect of undermethylation on mRNA cytoplasmic appearance and half-life. *Mol Cell Biol* 4: 538–543. PMID: 6201720
77. Schultz RM, Montgomery RR, Belanoff JR. (1983) Regulation of mouse oocyte meiotic maturation: Implication of a decrease in oocyte cAMP and protein dephosphorylation in commitment to resume meiosis. *Dev Biol* 97: 264–273. PMID: 6189752
78. Ma J, Svoboda P, Schultz RM, Stein P. (2001) Regulation of zygotic gene activation in the preimplantation mouse embryo: Global activation and repression of gene expression. *Biol Reprod* 64: 1713–1721. PMID: 11369600
79. Chatot CL, Ziomek CA, Bavister BD, Lewis JL, Torres I. (1989) An improved culture medium supports development of random-bred 1-cell mouse embryos in vitro. *J Reprod Fertil* 86: 679–688. PMID: 2760894
80. Tsafiriri A, Chun SY, Zhang R, Hsueh AJ, Conti M. (1996) Oocyte maturation involves compartmentalization and opposing changes of cAMP levels in follicular somatic and germ cells: Studies using selective phosphodiesterase inhibitors. *Dev Biol* 178: 393–402. <https://doi.org/10.1006/dbio.1996.0226> PMID: 8812137
81. Erbach GT, Lawitts JA, Papaioannou VE, Biggers JD. (1994) Differential growth of the mouse preimplantation embryo in chemically defined media. *Biol Reprod* 50: 1027–1033. PMID: 8025158
82. Kasowitz SD, Luo M, Ma J, Leu NA, Wang PJ. (2017) Embryonic lethality and defective male germ cell development in mice lacking UTF1. *Sci Rep* 7: 17259. <https://doi.org/10.1038/s41598-017-17482-z> PMID: 29222434

83. Reddi PP, Naaby-Hansen S, Aguolnik I, Tsai JY, Silver LM, et al. (1995) Complementary deoxyribonucleic acid cloning and characterization of mSP-10: The mouse homologue of human acrosomal protein SP-10. *Biol Reprod* 53: 873–881. PMID: [8547483](https://pubmed.ncbi.nlm.nih.gov/8547483/)
84. Li H, Handsaker B, Wysoker A, Fennell T, Ruan J, et al. (2009) The sequence Alignment/Map format and SAMtools. *Bioinformatics* 25: 2078–2079. <https://doi.org/10.1093/bioinformatics/btp352> PMID: [19505943](https://pubmed.ncbi.nlm.nih.gov/19505943/)
85. Anders S, Pyl PT, Huber W. (2015) HTSeq—a python framework to work with high-throughput sequencing data. *Bioinformatics* 31: 166–169. <https://doi.org/10.1093/bioinformatics/btu638> PMID: [25260700](https://pubmed.ncbi.nlm.nih.gov/25260700/)
86. Love MI, Huber W, Anders S. (2014) Moderated estimation of fold change and dispersion for RNA-seq data with DESeq2. *Genome Biol* 15: 550. <https://doi.org/10.1186/s13059-014-0550-8> PMID: [25516281](https://pubmed.ncbi.nlm.nih.gov/25516281/)
87. Huang da W, Sherman BT, Lempicki RA. (2009) Systematic and integrative analysis of large gene lists using DAVID bioinformatics resources. *Nat Protoc* 4: 44–57. <https://doi.org/10.1038/nprot.2008.211> PMID: [19131956](https://pubmed.ncbi.nlm.nih.gov/19131956/)
88. Lee JY, Yeh I, Park JY, Tian B. (2007) PolyA_DB 2: MRNA polyadenylation sites in vertebrate genes. *Nucleic Acids Res* 35: D165–8. <https://doi.org/10.1093/nar/gkl870> PMID: [17202160](https://pubmed.ncbi.nlm.nih.gov/17202160/)
89. Kurasawa S, Schultz RM, Kopf GS. (1989) Egg-induced modifications of the zona pellucida of mouse eggs: Effects of microinjected inositol 1,4,5-trisphosphate. *Dev Biol* 133: 295–304. PMID: [2785065](https://pubmed.ncbi.nlm.nih.gov/2785065/)
90. Yang F, Skaletsky H, Wang PJ. (2007) Ubl4b, an X-derived retrogene, is specifically expressed in post-meiotic germ cells in mammals. *Gene Expr Patterns* 7: 131–136. <https://doi.org/10.1016/j.modgep.2006.06.002> PMID: [16872915](https://pubmed.ncbi.nlm.nih.gov/16872915/)